POLITECNICO DI TORINO

in collaboration with

ÉCOLE POLYTECHNIQUE FÉDÉRALE DE LAUSANNE

Master's degree in Geotechnical Civil Engineering

Experimental Evaluation of Mechanical Characteristics of Steel-Bentonite Interface in Hygroscopic Conditions and Under Suction Control Conditions

Academic Supervisors:

Prof. Ing. Guido Musso, Politecnico di Torino

Prof. Ing. Alessio Ferrari, EPFL

Ing. Eleni Stavropoulou, EPFL

Candidate:

Fabiana Sannasardo

A.A. 2021-2022

Abstract

Deep geological repository is nowadays accounted as the most feasible choice for the storage of High-Level radioactive waste; it is the based on the idea of deep tunnel construction in which the waste will be emplaced and secured by a system of multiple barriers. As a common denominator of many different designs, it is possible to find the usage of bentonite backfilling, due to its beneficial properties, such as swelling potential. In nuclear waste repositories the pollution risk must be prevented ideally for a time window of thousands of years, thus the solution needs to be long term and needs to consider all the processes that will develop from the moment of emplacement to the farther future of the system. Specifically, the main processes that will certainly develop are: hydration of bentonite, due to water flow coming from the surrounding saturated host rock formation and heating, caused by the radioactive decay of the waste. The aim of this thesis is to increase the knowledge concerning the shear strength parameters accounting for the first of the two afore exposed processes. More in detail, the experimental campaign performed is divided into three parts, connected to each other; the first experimental step was the development of a feasible protocol to impose certain suction levels over bentonite samples, leading also to the possibility of reinterpreting the collected data to obtain part of the water retention mechanism; the second part is dedicated to a direct shear testing campaign, needed to evaluate the soil shear strength properties, with related attempts in effective stresses evaluation; last part will focus on the interface shear testing, using the "tools" exhibited in the previous parts, and allowing to then compare the interface behaviour with the one of the soil, under the imposed suction conditions.

Riassunto

Il deposito geologico profondo è oggi considerato la scelta più adatta ai fini dello stoccaggio delle scorie nucleari ad alto livello di radioattività; la sua realizzazione si basa sull'idea di costruire tunnel profondi in cui i rifiuti saranno collocati e messi in sicurezza grazie a un sistema di barriere multiple. In Europa molti paesi hanno sviluppato il proprio concetti di stoccaggio delle scorie nucleari, ciononostante è possibile individuare un comun denominatore fra i diversi concetti, ovvero l'utilizzo della bentonite come materiale di riempimento, grazie alle sue proprietà benefiche, come il potenziale di rigonfiamento. Il design del deposito geologico profondo ha come obiettivo la mitigazione della diffusione e del trasporto di agenti inquinanti per un tempo nell'ordine di migliaia di anni; perciò, la soluzione deve tenere conto di tutti i processi che si svilupperanno dal momento della posa in opera fino al futuro più lontano del sistema. In particolare, i principali processi che indubbiamente si manifesteranno possono essere sintetizzati nelle seguenti due voci: l'idratazione della bentonite dovuta al flusso d'acqua proveniente dalla formazione rocciosa circostante; il riscaldamento causato dal decadimento radioattivo dei rifiuti. Lo scopo di questa tesi è quello di accrescere le conoscenze relative ai parametri di resistenza al taglio, tenendo conto del primo dei due processi sopra esposti. Più in dettaglio, la campagna sperimentale svolta è suddivisa in tre parti, collegate tra loro; il primo step è stato lo sviluppo di un protocollo per l'imposizione di determinati livelli di suzione su campioni di bentonite, consentendo inoltre la reinterpretazione dei dati raccolti per ottenere parte della curva di ritenzione; la seconda parte è dedicata a una campagna di prove di taglio diretto necessarie per valutare le proprietà di resistenza al taglio del terreno con relativi tentativi di valutazione delle tensioni efficaci; l'ultima parte sarà dedicata alle prove di taglio di interfaccia, utilizzando quanto appreso dalle parti precedenti e permettendo quindi di confrontare il comportamento dell'interfaccia con quello del terreno, nelle condizioni di suzione imposte.

Contents

Introduction

After more than 70 years of nuclear plants usage for electricity generation, large amounts of nuclear waste have been accumulated worldwide.

According to the last adjournment published by the World Nuclear Association, the energy consumption is estimated to be doubled in the next twenty years; nowadays the share of nuclear power produced energy is about 10% worldwide and 18% in the OECD countries (Organisation for Economic Co-Operation and Development).

The aim of this experimental investigation is related to the latest interest in Bentonite as buffer material for Deep Nuclear Waste Disposal; a scheme of the deep Geological Repository is reported in *Figure 1.1*. The buffer is the material positioned in between the host rock and the steel canister; it will be involved in very complex processes, thus the need to gain experimental data to be used for model calibration, allowing for prediction of the system's behaviour, accounting for the changes of mechanical characteristics of the involved materials in the long-term.

It is known that the buffer material will be firstly saturated by the host rock and secondly submitted by heat coming from the nuclear waste contained in the canister.

Therefore, it's fundamental to understand the evolution of bentonite's mechanical properties, which is the chosen material in the Swiss Nuclear Waste Disposal concept, regarding the variation of water content.

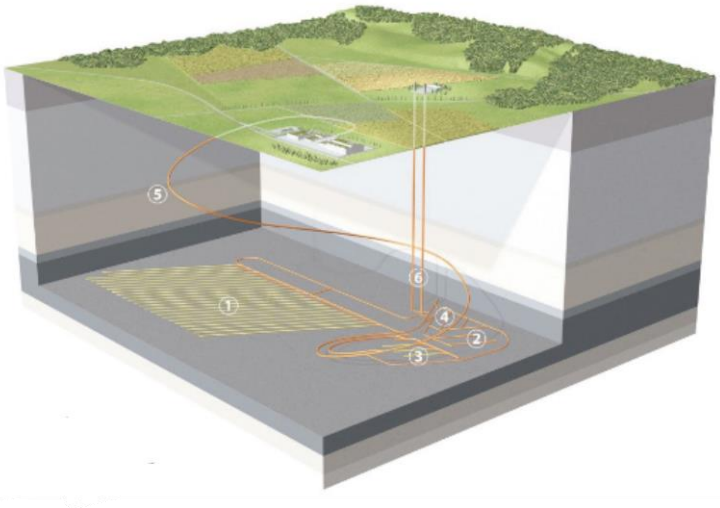

Figure 1.1 – Deep Geological Repository (Source: Modified by Swiss Federal Office for Energy)

This thesis is developed according to the Swiss regulations, hence the soil studied is bentonite that as afore mentioned will play the role of buffering material, with two principal aims:

- Experimental evaluation of shear strength variations according to the above reported environmental imposed conditions, such as suction imposition to the soil and then shear strength evaluation through direct shear testing
- Experimental evaluation of interface shear strength variations under the same imposed environmental conditions

In the following the outline of the thesis is synthesized:

The *first chapter* will be dedicated to literature review of the nuclear waste disposal concepts, concerning the expected changes of the boundary conditions and the interactions between buffer and steel interfaces.

The *second chapter* will be dedicated to literature review of the state of the art concerning bentonite, an overview of the chemical and mechanical properties of bentonite will be given. Then two in situ full scale tests will be described together with conclusions derived from them.

The *third chapter* will be dedicated to a theoretical framework on hydraulic properties of the soil, definition of suction and his influence over the evaluation of effective stresses, according to different formulations.

The *fourth chapter* will be dedicated to the explanation of experimental procedure adopted for suction control, starting from sample preparation, with illustration of the different approaches considered and the final protocol used. In the final part of the chapter, it is shown a brief attempt to fit the experimental water retention curve through simple mathematical formulations.

The *fifth chapter* will be dedicated to the experimental campaign for shear strength evaluation under suction control, starting from the characterization of the tested material, the calibration process for the shearing procedure and the calibration process for shearing under controlled suction condition, till the final elaboration of test results.

The *sixth chapter* will be dedicated to the experimental campaign of steel-bentonite interface shear strength evaluation, under suction control. An explanation of the different setup will be given together with problems encountered and elaboration of the tests results.

1. Literature review

1.1 Nuclear Waste Disposal Concepts

Most of the contemporary concepts concerning Nuclear Waste disposal took inspiration from the quality standard set by the Swedish KBS project developed in the late 70s.

According to the "World Nuclear Waste Report" (2019), the approach was based on the multibarrier system, describes as the Russian doll principle, meant to ensure the containment of the radioactive waste.

The idea behind deep geological disposal is concretized in the concept of engineered barriers (EB), meaning that different soil-layers will surround the canister (being a barrier itself) containing the nuclear waste, with the purpose of minimizing the risk of radioactivity release in the biosphere.

More in detail, the deep geological disposal will be realized at great depth in specific geologic formations, called Host Rocks, and that will constitute the first geological barrier. Galleries will be realized, with a main central corridor connecting multiple secondary tunnels, each designed to contain the canister; disposition and geometry of the secondary tunnels change in the different countries' concept of nuclear waste disposal.

Nowadays the formations investigated to fit as host rock are mainly salt formations, granitic rock and claystones. Some countries concepts are very similar, i.e., the Spanish concept differs from the Swiss only for the host rock chosen, while some others differ also in the geometries used, for example in the French concept there will be no buffer, tunnels will be filled with concrete for medium-level nuclear waste, whilst the High-Level nuclear waste will be stored into small tunnels with a steel lining.

Although the final disposition of nuclear waste is accepted worldwide to be the deep geological repository, the waste itself will go through a preliminary process, to reduce the radioactive hazard. It can be synthetized into the following bullet points:

- reprocessing – process in which some still usable fuel elements are extracted from the used waste;
- vitrification - process of solidification of the waste in a borosilicate glass layer;

- encapsulating and transportation to interim storage facilities.

A simplified scheme of the process is reported in *Figure 1.2*.

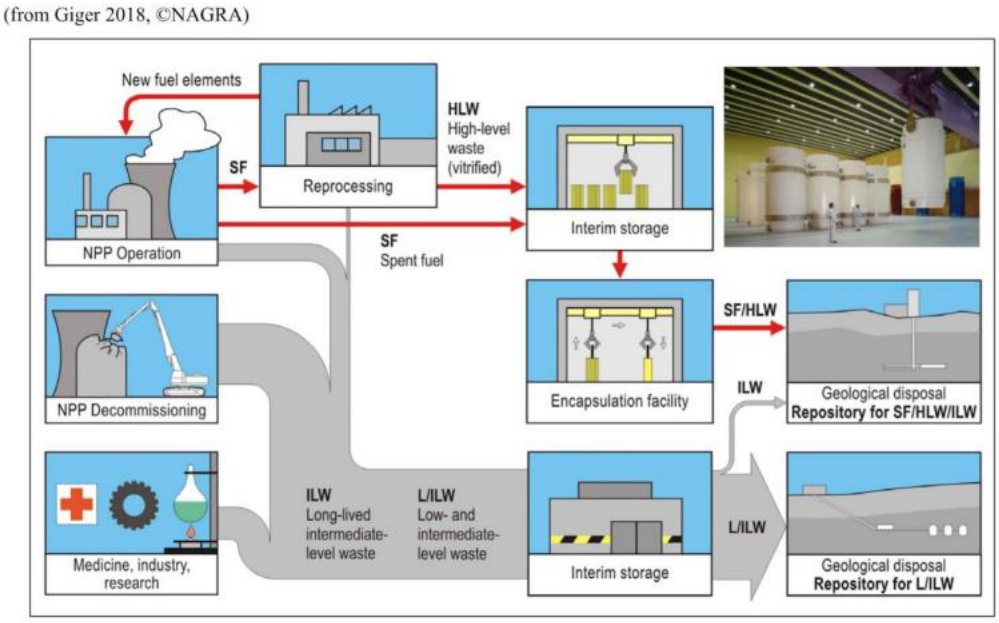

Figure 1.2 – Nuclear waste cycle for medium and high level nuclear waste (Source: Nagra)

In the following two different nuclear waste disposal concepts will be described.

1.1.1 Swiss Concept

The Swiss concept can be described as a multi-barrier system, schematized in *Figure 1.3*.

The system of galleries will be realized at great depth (500-1000m), with a principal corridor allowing the access to the secondary galleries. Each secondary gallery will be realised considering the steel canister radius plus one meter as reference for the design radius, the extra meter allows the emplacement of the bentonite buffer. Therefore, the steel canister will be positioned at the centre of the gallery and his weight will be held by compacted blocks of bentonite, the remaining space between canister and host rock walls will be filled with granular bentonite backfilling.

What just described represent a system of 3 barriers, the third and last barrier will be a stable deep formation, that in the Swiss concept is the Opalinius Clay.

This EBS (Engineered Barrier System) may seem very simple in his realization but hides a high level of complexity that require robust and validated numerical tools to predict long term response of the system itself. Indeed, the time scale of the problem to study is in the order of thousands of years, therefore the feasibility of the disposal needs to be studied considering the changes that over this period the materials involved will deal with.

Figure 1.3 – The Swiss concept of deep geological storage of SF/HLW (Source: Modified from NAGRA, 2019).

The Swiss Confederation has given Nagra, which is the National Cooperative for the disposal of radioactive waste, the mandate to plan and realise a deep geological repository.

1.1.2 Italian concept

The nuclear waste today present in Italy not only comes from the past season of electric energy production but also from research activity conducted in some plants. The Italian nuclear plants were functioning between the 50s and the 80s and they were all shut down after the National Referendum that took place in 1987.

Immediately after, a company called Sogin was entrusted by law to manage with the nuclear fuel produced in the Italian power plants. The strategy adopted by Sogin for fuel management follows the guidelines formulated by the Italian Government.

The concept of disposal designed by Sogin has the final goal of realizing the national repository. The national repository is a surface environmental infrastructure based on multi-barrier system, where radioactive waste can be safely disposed of.

This will allow the disposal of approximately 78 thousand cubic metres of VLLW (very low level waste) and LLW (low level waste) and the long-term interim storage of approximately 17 thousand cubic metres of ILW (intermediate level waste) and HLW (high level waste).

This multibarrier system is composed by four levels, reported in the following:

1. Steel Canister, where radioactive waste conditioned is immersed in a cementitious matrix
2. Module, concrete boxes where the canisters will be emplaced, designed to withstand 350 years
3. Cell, a second bigger reinforced concrete box where the modules will be inserted
4. Multilayer hill, artificial structure arranged to cover the cells, built in such way to prevent infiltration of rainwater and isolate the waste

A scheme of what described is reported in *Figure 1.4*.

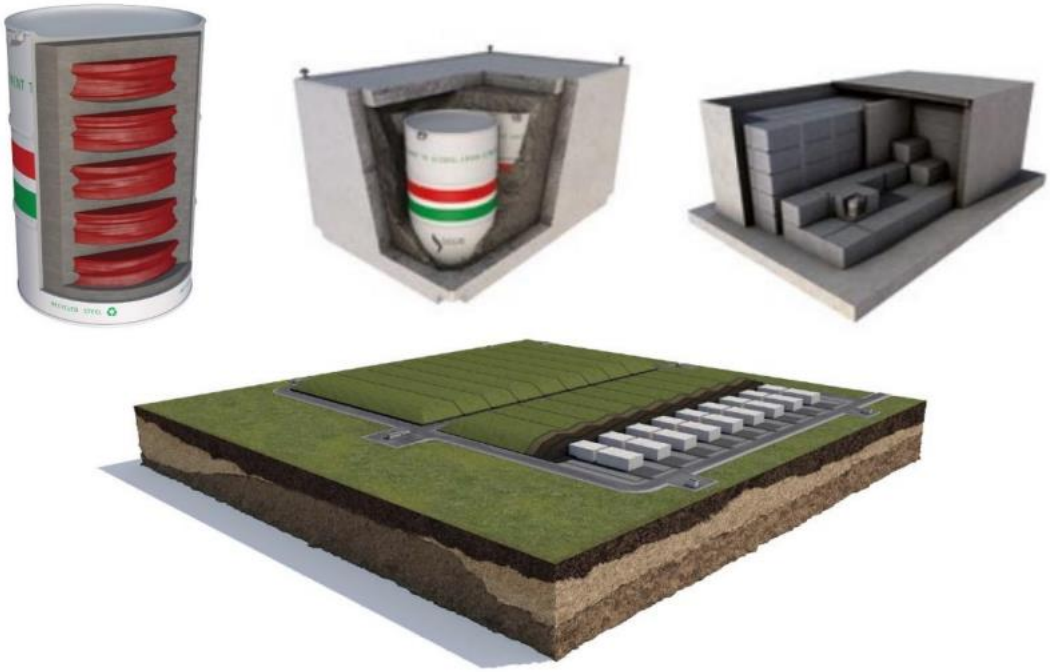

Figure 1.4 – (a) steel canister containing layers of vitrified nuclear waste immersed in cement matrix; (b) module containing several steel canisters; (c) cell containing several modules; (d) representation of the national repository (Source: Sogin official site)

Information reported above are taken from the official site of the company in charge; no precise information about material involved or site realisation is given.

1.2 Involved Multi-Physical Processes in Nuclear Waste Disposal

When dealing with Nuclear Waste Disposal, the concept of coupled analysis needs to be well understood, since the engineered barrier will go through several processes that will involve thermodynamics, both hydraulic characteristics of the soil and water flows and mechanics.

In *Figure 1.5* the reported illustration depicts a synthetic scheme of main processes that the tunnel will encounter, from t_0 - which can be addressed as the moment of tunnel realization - till t_∞.

The first step represents the excavation of the gallery, at this stage the saturated host formation walls will be exposed to the atmospheric pressure and so at the boundaries the

ventilation will bring desaturation; in this phase it's crucial to avoid the formation of an Excavation Damage Zone, phenomena that will be described later (paragraph 1.2.1). Then at the centre of the tunnel, the steel canister will be positioned over bentonite compacted blocks, and the rest of the space will be filled with granular bentonite. Once the system will be again closed, a process of re-saturation caused by capillary forces will begin, the water present in the host rock will travel to reach the bentonite buffer and blocks. In the last illustration on the right side, is represented the long-term condition, where a gas front will develop from the nuclear waste due to the canister corrosion, concurrently to heat emissions caused by the radioactive waste decay.

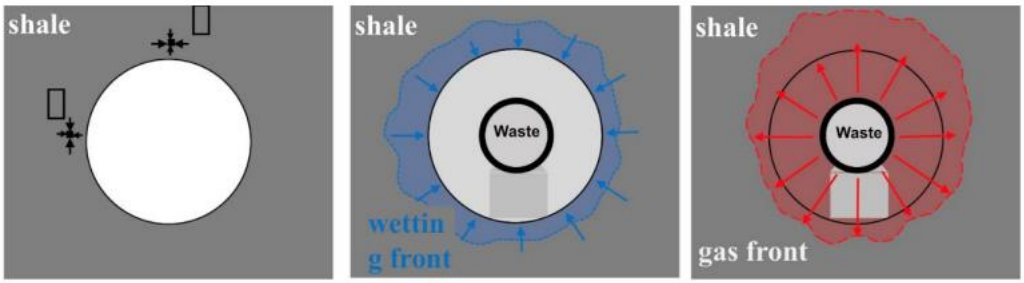

Figure 1.5 – Main phases of deep repository tunnels

The term "coupled processes" stands for processes that are interdependent, so a change occurring in one of them impacts directly and indirectly the others. Thermo-Hydro-Mechanical and Chemical coupled processes (THMC) are acknowledged to have a significant long-term impact on the three-barrier system and are widely recognized to be of critical importance on post-closure safety of GDFs (Geological Disposal Facility).

Specifically, the host rock formation chosen in the Swiss concept, OPA, appears to be full of faults, therefore things such as preferential paths are fundamental to be accounted for in the modelling process.

As mentioned before, bentonite will be emplaced in unsaturated state and will be hydrated by the groundwater flow of the host rock. The design hygroscopic water content will be around 5-6% and the relative humidity around 35-45%, with total suction in a range between 100-200MPa.

In confined condition, the progressive saturation of the buffer upon uptake of water from the host rock will be followed by the expansion of the bentonite and the consequent filling

of technological gaps in the systems. According to the wetting front that will developed, swelling will first occur at the boundaries, this will lead to the formation of a density gradient where the external areas will result in lower densities, since bentonite will be "free" to swell, and higher densities in the more internal areas where bentonite will be compressed. To look at the same problem from another prospective, it can be added that as the bentonite progressively saturate, the compression for the inner layers will occur at high suction levels whilst for the external layers the compression will happen at low suctions (Villar and Lloret, 2008).

As before represented in the illustration in *Figure 1.5*, eventually bentonite will be subjected to heating caused by the nuclear waste decay, leading to possible desaturation of the inner parts of the buffer. Hence, when analysing the hydraulic properties of bentonite, one fundamental characteristic to acknowledge is the Soil Water Retention Curve, that defines the behaviour of the soil in terms of wetting and drying path.

Nevertheless, it remains unclear whether the high temperatures around the canister would hinder the full saturation of the inner part of the barrier or just delay it. (Villar et al., 2016)

1.2.1 Excavation Damage Zone

The excavation damage zone, as the name preannounces, it's a time dependent phenomenon originated during the tunnel excavation and refers to the region where irreversible deformation involving crack propagation has developed. It leads to very severe consequences if not considered in the design stage of every kind of gallery, but especially in Nuclear Waste repositories, since leakage leads to pollution of the surrounding soil and groundwater.

During the tunnel excavation, two zones may develop (Blümling et al., 2007):

- An excavation disturbed zone, EdZ, where the hydromechanical modification occur without major changes, resulting in a zone that can still be defined safe

- An excavation damage zone, EDZ, where the hydromechanical modification leads to significant changes, resulting in the creation of an instable zone

In the context of nuclear waste repositories in crystalline rocks, regardless the need to predict the failure depth for safety management along the excavation stage, what is critical is the acknowledgment of EDZ properties of the host rock formation, since it can have severe implications in the performance.

Many numerical models have been developed in the attempt of predicting the evolution and extension of the EDZ, some of them were validated thanks to the data set obtained by Mont Terri experiment (Marschall et al., 2017), a representation of the conceptual model of the EDZ and actual cracks are reported in *Figure 1.6*.

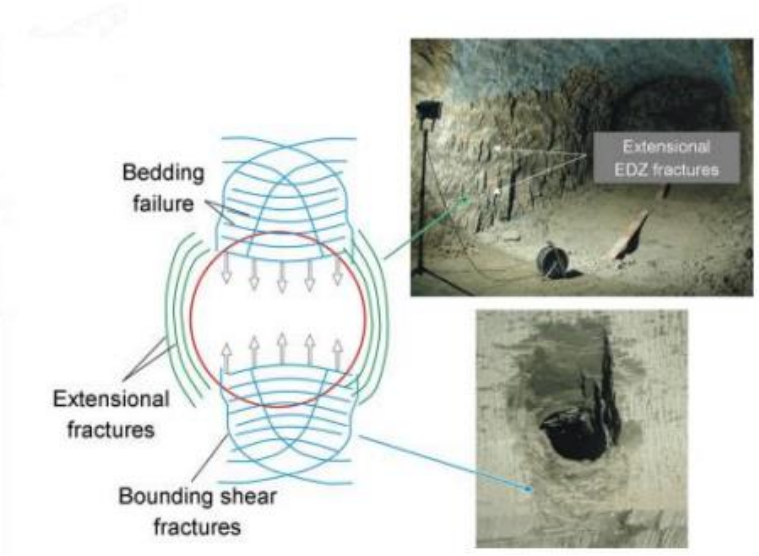

Figure 1.6 – Model and real EDZ in Mont Terri laboratory (Source:(Marschall et al., 2017)*)*

1.3 Soil-Steel Interface

Unsaturated interface conditions are common to many geotechnical engineering projects.

In general, the interface shear resistance developing between fine graded soils and structural surfaces will depend on the drainage conditions, in which the phenomena occurs (Subba Rao et al., 2000).

The usual investigation method of soil-structure interfaces goes by the use of direct shear box testing, thanks to the possibility of a rather easy modified setup of the box. The outcoming results were proven, by numerical modelling, to be similar to in-situ

conditions, even though in the past the approach was criticized due to impossibility of assuring the homogeneity of the soil stress state (Miller and Hamid, 2005). Furthermore, if one considers this interface setup purely as a surface test, homogeneity problem can be overcome, since homogeneity is required only along the idealized shear band.

Friction between soil and steel over the years has been widely studied, being an important phenomenon in geotechnical engineering. Also, in the Nuclear Waste Disposal contest, the canister lifetime will depend on the prevailing corrosion mechanisms and rates, the applied mechanical stresses in the evolving environment of the repository, and the evolution of the canister material properties.

However, very few have tried to integrate the processes and phenomena observed experimentally in the corrosion of the steel surface with the evolution of the surrounding bentonite properties in a conceptual framework.

In the following paragraphs an overview of the factors that influence the mechanical response of the soil-steel interfaces is given.

1.3.1 Steel Roughness

It is easy to imagine that steel roughness will have a major contribution to the shearing response of the counterpart, being the soil. Surface roughness is a measure of the texture of a surface. It is quantified by the vertical deviations of a real surface from its ideal form. If these deviations are great, the surface is rough, if they are small, the surface is smooth.

The roughness of a surface has most commonly been measured by an instrument in which a stylus travels across the surface, the movement of the stylus is amplified and the signal recorded. The result is generally expressed as Ra (average roughness) expressed in micrometers.

For the reasons priorly exposed, in the past decades several researchers have investigated the behaviour of soil-steel interfaces; for instance, Hamid and Miller (2009) have conducted extensive experimental investigations to study the interfacial interaction between the unsaturated silt-steel interfaces with rough and smooth surfaces. The authors found that the interface with rough finish exhibits more shearing resistance when

compared with the smooth steel counterface. However, the shear strength of soils was found to be greater than that of interfaces under similar stress state conditions.

According to Kishida and Uesugi (1987) the friction behaviour of a soil cannot be considered independent from the grain size of the soil in contact with the surface, thus the authors introduced a concept that is the normalized surface roughness (Rn) of the counterface, allowing to scale the steel roughness relatively to the grain-size diameter corresponding to 50% of the finer:

$$R_n = \frac{R_{max}}{D_{50}} \tag{1.1}$$

Where R_{max} is the steel roughness.

With the purpose of understanding the scale roughness considered when dealing steel counterfaces, in *Figure 1.7* are reported some examples of typical surface profiles of steel specimens.

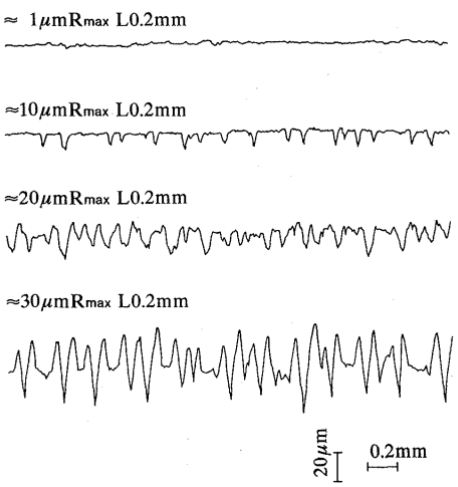

Figure 1.7– Typical roughness range for steel surfaces (Source: Tsubakihara and Hideaki, 1993)

Tsubakihara and Kishida (1993) demonstrated that for clays tested with simple shear type apparatus under constant pressure conditions, shear strain at the peak strength increased with the increment of steel roughness.

The same authors concluded after a trial of tests under different steel roughness conditions that: whenever the steel surface is smoother than the critical roughness, sliding occurs at the clay steel interface. The maximum resistance of friction increases with the increment of steel roughness; the maximum resistance of friction is upper-bounded by the shear strength of the soil.

From Porcino et al., (2003) the same conclusion was drown from interface testing performed through direct shear tests on a Toyoura dense sand; the same year Sun et al. (2003) through direct shear testing concluded, for different specimens having different clay percentages, that the surface friction resistance at peak and residual increase with increasing steel surface roughness, concluding that shear failure occurs within the soil when the roughness of the interface is rather large.

Later on Hu and Pu (2004) introduced the concept of critical roughness, which allows to predict the failure mode if compared with the relative interface roughness; for a R_n value smaller than R_{cr} (smooth interface) the expected interface shear failure is elastic perfectly plastic with little dilatancy at the interface, whenever R_n value is higher than R_{cr} (rough surface) what is expected is a shear failure coupled with strain softening and strong dilatancy.

1.3.2 Mean Particle Size

As mentioned before, particle size is used as a scaling factor to the steel surface roughness.

From Su et al. (2018) was reported that the interface friction angle increases with R_n till an upper bound limit, that was afore mentioned as R_{cr} , from which it will decrease again. From the authors was also stated that D_{50} has no direct influence on the friction angle value obtained for the interface, but rather an indirect influence due to its usage as a scaling factor.

However, during the same experimental campaign the authors investigated the behaviour of the soil through regular shear testing, and found a direct relationship between D_{50} and friction angle, specifically an increasing value of friction angle with increasing value of D_{50}.

If one imagines studying the soil particles laying on the shearing band, the bigger the particle the more probable is the presence of defects, leading to a higher probability of particle breakage while shearing occurs.

As the shearing continues, the amount of bigger particles will decrease thus the amount of smaller particles will increase; when particles will reach basically an average size they will simply move to fill the voids during the shearing process, leading to a specimen densification. The process just described is reported schematically in *Figure 1.8,* and affects the shear strength of a granular system.

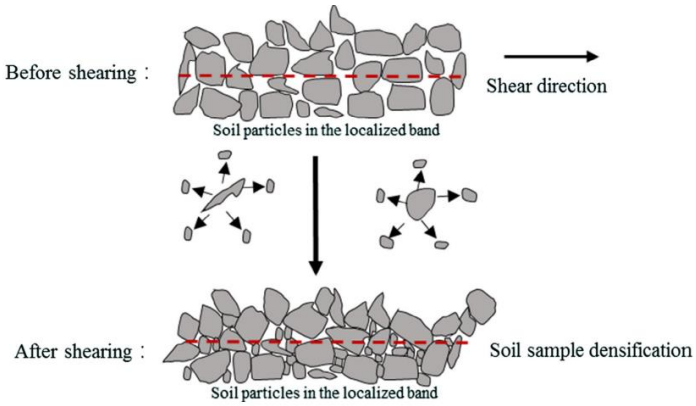

Figure 1.8 – Particle breakage and soil densification occurring in a soil sample while shearing (Source: Su et al., 2018)

The same process but with a steel counterface leads to different results, in particular the particles breakage is less likely to occur with such shearing configuration, hence the influence of D_{50} on friction angle is lower (Su et al., 2018).

Another aspect linked to particle breakage is shearing rate. His influence on the shearing response for soil-steel interface was investigated by Sun et al. (2003), through direct shear testing on different soil samples. More in detail, the interface testing was conducted over silty and clayey soil samples and the conclusion derived were: no influence of the investigated shear rates could be found in mainly silty soils, whilst with increasing clay percentage a contribution to shear strength was given at peak, if increasing the shear rate.

1.3.3 Corrosion

The last factor considered in the soil-steel interface study, is the corrosion phenomena. The reasons behind this evaluation can be simply addressed to the awareness of the saturation process that will involve the soil surrounding the steel canister.

Consequently, to the backfilling and the sealing of the tunnel, aerobic conditions will bring aerobic corrosion of the metal due to oxidation phenomena, in the meantime due to microbial activity with oxygen consumption, anoxic conditions might develop locally.

The consequence of anaerobic corrosion is the formation of mobile iron species that through interaction with clay minerals will form iron-rich particles, those will precipitate in the surroundings of the interface between the two involved materials.

Some samples extracted from Mont-Terri Full-scale experiment have shown (Leupin et al., 2021) the formation of a reddish corrosion front, that can be attributed to the concentration of iron in the bentonite matrix. In the following a brief explanation of each boundary stage reported in *Figure 1.9* is given:

a. Water coming from the host rock will saturate bentonite and will diffuse towards the steel canister
b. In such anaerobic conditions iron will be corroded, producing magnetite and Fe^{2+} ions. These ions will diffuse within the bentonite buffer with the creation of an iron enriched zone
c. The diffused ions of Fe^{2+} will be oxidized by the residual O_2 present, leading to corrosion products such as Fe (III), that will precipitate.
d. This process brings to high rate of water consumption and the H_2 produced leads to microfractures since the hydraulic conductivity of saturated bentonite is low
e. The still ongoing process described in point c will lead now to precipitation of these ions into the paths created by the cracks
f. As the layer of precipitated ions grows bigger the corrosion rate decreases and bentonite can resaturate, although loses its self-healing capacity along this microfractures walls

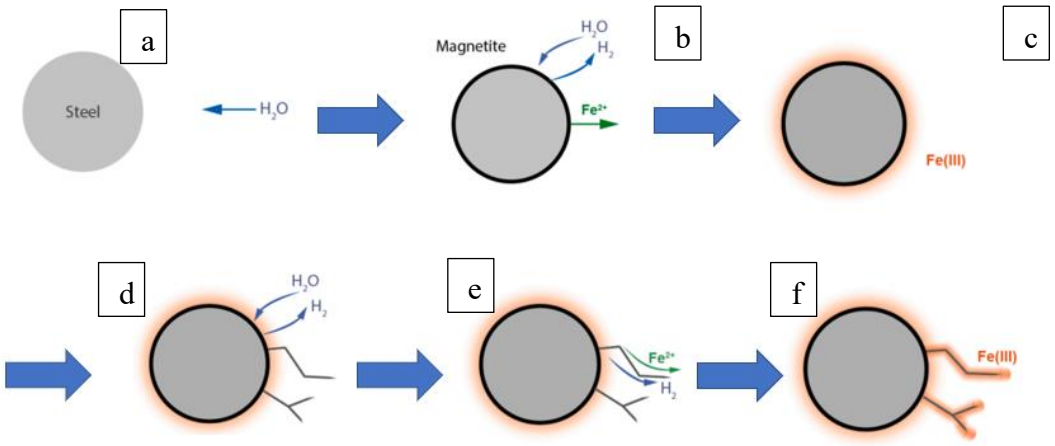

Figure 1.9 – Interaction between carbon steel and bentonite (Source: Modified by Leupin et al., 2021)

Other samples coming again from Mont-Terri in situ experiment were analysed by Reddy et al. (2020), among all the investigated aspect the corrosion rate obtained was an average value of 1-2 micrometres for year.

Another general conclusion derived by all the afore mentioned researchers and also from Smart et al. (2017) is that the corrosion rates are higher in the case of bentonite pellets around the steel canister, if compared with the ones obtained with compacted bentonite blocks.

2. Bentonite as a Sealing Material: State of the Art

2.1 Reason of Interest

The buffer barrier was firstly introduced by the SKB concept of nuclear waste disposal, and in the development happened over the years, looking for the suitable material to fulfil the purpose, some mechanical and hydraulic characteristics have been declared fundamental for safety and functioning of the barrier.

What was researched was a material capable of withstanding high temperature gradients, isolating the HL nuclear waste, acting as a self-healing barrier against water channels; preventing from leakage of radionuclide contaminated water and lastly from a pure tunnelling engineering point of view, capable of mitigating stresses caused by creeps at the boundaries.

The reasoning behind the decision of bentonite usage as buffer material in the Swiss concept can be found in the suitability of this material if compared with the requirements before mentioned, i.e., bentonite has been now studied for decades and its properties can be synthetized in the following points:

- Low permeability

- High swelling potential

- Low hydraulic conductivity

- Self-healing capacity

Of course, no such thing as a perfect material/soil exists for the purpose, therefore bentonite has also characteristic that make rather complex and difficult to predict the long-term evolution of some fundamental properties, like shear strength, if coupled with boundaries changes that the barrier material is supposed to encounter.

2.2 Bentonite Characteristics

It is possible to define bentonite as those clays that are rich in smectite minerals. A visual representation at different scales of bentonite is reported in *Figure 2.1*. In the left picture there is a schematic representation of the basic structure of smectite (montmorillonite) minerals composed by the silica (Tethaedral) -aluminium (Octahedral) -silica (Thetahedral); (TOT) structure and the interlayer water adsorbed to the exchangeable cations that compensate the electrical charge on the surface.

The presence of smectite minerals, with a high isomorphic substitution, leads to high presence of cations in the external surfaces. These positive charges increase the interaction between clay particles and pore fluid, leading to different concepts of water storage in the soil. Specifically, water in bentonite is stored according to an additional mechanism to the classic adsorption, which is interlayer adsorption. This interlayer water will have different properties from the free water, showing characteristics like viscosity.

In the middle illustration there is a qualitative representation of the microstructure of bentonite, where is possible to highlight that smectite particles tend to stay close to each other, this mechanism gets truer with decreasing water content and so increasing suction value, whilst they will tend to shift apart as the pore water potential decreases.

Also, another phenomenon involving bentonite is known as oversaturation, which means that soil is capable of storing more water than the amount corresponding to its standard (bulk) pore space (Michalec et al., 2021). This is linked to the above briefly explained inner structure and chemistry, in particular to the percentages of the Montmorillonite mineral.

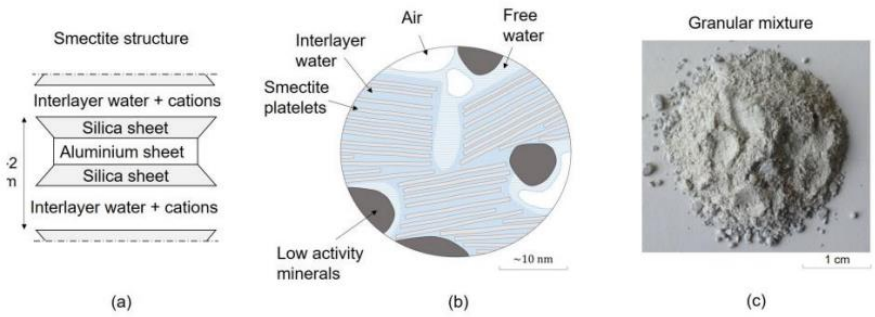

Figure 2.1 – 3 different scales of bentonite (Source: Bosch, 2021)

The third image (c) represents the fabric of bentonite that will be used as buffer, therefore a granular mixture in unsaturated conditions, with designed grain size distribution and dry density.

Usually, according to suction levels, it's possible to differentiate the structure of bentonite into (Zhang et al., 2020):

- Three molecular layers of water, for suction under 7MPa
- 2 molecular layers of water, for suction 50<s<7MPa
- One molecular layer of water, for suction above 50MPa

The governing pore water storing mechanisms will be osmotic for saturated conditions, corresponding to low suction levels, and capillary mechanisms for high suction levels.

Since smectite particles have high capacity of water absorption, this will result in a high swelling potential. This characteristic indeed enhances the self-healing of fractures that may develop in the tunnels and permit to limit the radioactive activity; his low capacity is a fundamental characteristic to isolate the radionuclides and forbid their diffusion.

In the following are reported few bentonite parameters/properties, retained to be relevant to the purposes of soil characterization.

2.2.1 Target dry density

The granular bentonite will be emplaced at a target dry density and will be in confined conditions. However, the development of a density gradient in the system is inevitable, due to the waterfront development from the host rock to the buffer.

The density gradient may be established with lower densities in the areas where the bentonite can expand, and with higher densities in the internal areas where the bentonite is compressed.

Whenever speaking about dry density variation, a reflection in void ratio values can be expected. By an analysis performed by Villar (2007) it was highlighted that little influence of the void ratio can be foreseen in the water retention curves, plotted in terms of suction vs. water content, for materials like FEBEX and MX-80 bentonites whenever

in a range of suctions higher than 10MPa. Whilst if we reason in terms of degree of saturation to plot the WRC, it is possible to see the curves shift between each other as a function of the void ratio (Seiphoori et al.,2014), highlighting that the degree of saturation is affected by the grain size distribution of the fabric and by the loading and volumetric conditions under which the wetting/drying paths take place.

The relevance of the dry density is linked to its intimately relation with the swelling potential, therefore some past researches have investigated the swelling behaviour of bentonite under constant volume condition, so that "e" value could be considered as dead parameter, and found out that upon wetting the relation between swelling pressure and dry density is exponential (Villar & Lloret, 2008).

2.2.2 Activity

With the term bentonite one can refer to any material whose primary components belong to the smectite group of minerals, therefore to a soil where physical properties are controlled by the smectite minerals. Among the principal characteristics of smectite minerals, it is possible to name the large cation-exchange capacity, a great specific surface area, very high swelling potential, low permeability and low hydraulic conductivity to water.

Bentonite is defined as a clay with a high activity, where the activity of a clay can be defined as the ratio between the plasticity index and the clay fraction. The higher the plasticity index the more pronounced are the colloidal properties of the clay.

In *Figure 2.2* is reported a schematization of the microstructure of a bentonite particle, with two silica tetrahedral sheets and one aluminium octahedral sheet (TOT). In between the two silica sheet is reported a layer of "solid water", intended as a thick film of water characterized by a very ordered structure and with a distance from the clay mineral surfaces lower than 1nm. Other kinds of water layer can be identified depending on the distance from the clay mineral surfaces, we refer to "liquid water" when such distance is higher than 1nm but we still have ions interaction; we refer to "bulk water" or "free water" when the distance is high enough not to have any effect of ion balancing with the clay surfaces. As before said, the main mineral group in bentonite clay is smectite group and

the main mineral is montmorillonite, which has high isomorphic substitution characteristics.

Inside what is represented as Diffuse Layer in *Figure 2.2*, ions are defined as non-movable, whilst in the external water, the bulk water, ions are free to move.

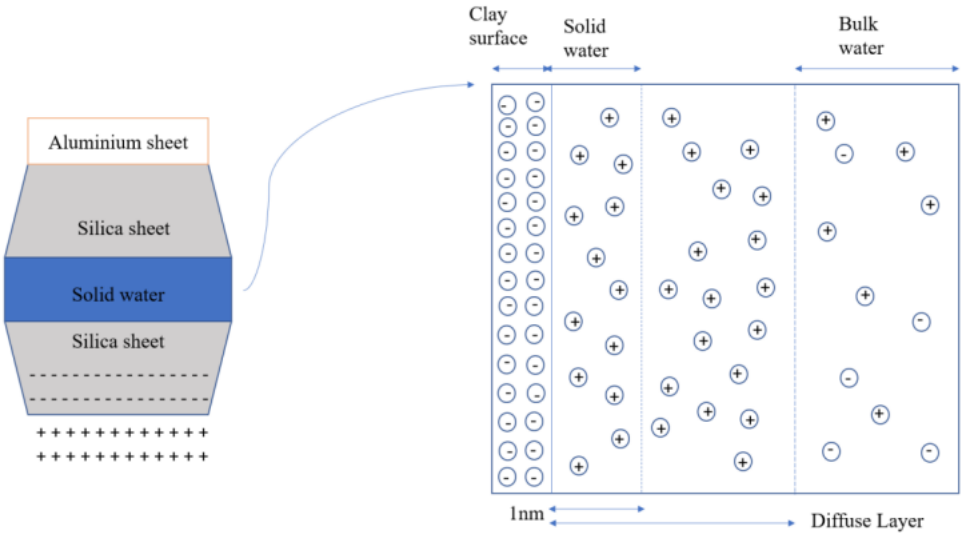

Figure 2.2 – TOT structure of bentonite and water interaction (Source: modified by Tuttolomondo, 2021)

2.2.3 Sodium vs Calcium Based

A common first differentiation among bentonites can be done basing on the dominant exchangeable cation, leading to a classification into either sodium or calcium based bentonites. The first one is the chosen candidate for nuclear waste disposal due to its superior swelling capacity. Indeed, the calcium based bentonite has smaller swelling capacity and higher conductivity to water.

Nonetheless some researches have suggested that calcium based bentonite may be more stable if exposed to chemical constituents travelling inside fluids (Gleason et al., 1997).

More into detail, the meaning of Sodium and Calcium based bentonite derives from the principal ion exchanger. In sodium montmorillonite the water adsorption mechanism is governed by Na+ ion, which has a high tendency to water adsorption; where in sodium

bentonite the adsorption mechanism is governed by Ca+ ion, which is chemically less susceptible to water adsorption (Muhammad & Siddiqua, 2022).

Unfortunately, it is very likely that sodium-bentonite undergoes ion exchange, transforming into calcium based bentonite, due to the calcium content of most soils being enough to activate such process (Dananaj et al., 2005). As a consequence of the transformation certain reduction in volume due to the decreasing distance between the montmorillonite flakes and a loss of water of approximately 6-12% can be observed (Egloffstein, 2001), as reported in *Figure 2.3*.

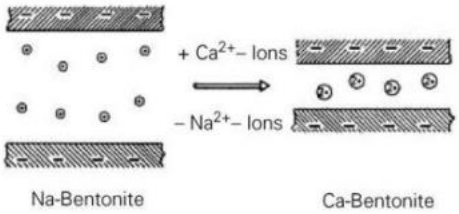

Figure 2.3 – Water reduction due to ion exchange (Source: Egloffstein, 2001)

2.2.4 Carbonate Content

Another contribution to the mechanical behaviour of clays is given by their carbonate content. In particular, many research have been conducted in the past bringing to the output that carbonate content can deeply influence the mechanical properties of a clay (Del Olmo et al.,1996).

This content can vary significantly in a clay formation, but an upper threshold value was proven to exist, above which the increase in carbonate content does not affect the strength of the interparticle cement bridges developed, leading just to a filling of the interparticle voids (McKown and Ladd, 1982). Indeed, it is considered that a percentage of the carbonates present inside the soil will precipitate in the point of contact between particles, leading to the formation of the afore mentioned cement bridges, which result in a strong bonding (Fukue et al., 1999).

In the context of nuclear waste disposal, the coupling among carbonate content and thermal gradient needs to be considered, since thermo-plastic strains strongly depend on

carbonate content. More specifically, the higher the carbonate content, the lower are the thermos-softening effects observed in the clays (Hueckel and Baldi, 1990).

In the final configuration of the deep repository, it is known that a heating phase will take place, during which a gradient of pore pressure will develop, leading to an increase of the natural water flow. At deviatoric stress, this same increase can lead to failure and or hydraulic fracturing (Hueckel and Pellegrini, 1992). The pore pressure build up is a consequence of the different thermal expansion between pore water and thermal volumetric strain of the solid skeleton. From experiments was deducted an almost linear peak strength reduction with temperatures up to 120 °C, a strong dependence of thermos-plastic strain with carbonate content and lastly no influence on the ultimate strength was found. (Hueckel et al., 1998)

2.2.5 Swelling

To understand the physical meaning of swelling and his stress dependency, let's imagine to wet under constant total stress a soil sample; for low stresses the material will swell, but if we increase the stress the same material will encounter a first swelling followed then by a significant volume decrease. If now the same behaviour is studied at the microscopic level, it's possible to imagine that when the stress is firstly applied, the response will be the creation of shear and normal forces at the particle contact. If increasing the ratio between these two forces, it will exceed the inter-particle friction angle and the natural output will be slippage between particles. The consequence of the slippage, at the particle point of contacts, results in overall compression of the unsaturated media.

In unsaturated media the presence of menisci between particles gives additional contribution to the resistance of the soil to the applied external stresses, therefore this stabilising effect will limit the decrease in volume. If in this condition we lower the suction value, therefore we increase the pore water pressure, the result will be that menisci close to each other will become one, and the final output will be volume increase (Tarantino, 2010).

The swelling potential of bentonites is counted as one of the main characteristics that make this soil the chosen candidate for buffering material. Therefore, understanding the hydromechanical behaviour of bentonite in terms of swelling, is an essential key point for analysing the long-term performance of the repository system.

The hydro-mechanical behaviour of compacted swelling clays with regard to the swelling capacity and compressibility behaviour at ambient temperature has been studied by various researchers for over more than 30 years now (Bucher and Mayor, 1989; Komine and Ogata, 1994; Delage et al.,1999; Villar, 1999; Lloret et al, 2003; Cuisinier and Masrouri, 2005; Hoffmann et al., 2007; Villar and Lloret, 2007; Nowamooz and Masrouri, 2009; Nowamooz et al., 2012; De'an Sun et al., 2014; Takayama et al., 2017; Zhao Zhang et al., 2020; Jean-Claude Robinet et al, 2021).

A common conclusion from these works is that suction has an important influence on the mechanical properties of the swelling material. In general, it has been reported that the heating may result in the expansion of the saturated clays under low stress of high overconsolidation ratios. From Tang et al. (2008) was reported that the overconsolidation ratio and the total suction are found to be the parameters affecting the thermal volumetric response of bentonite the most.

In Bosch (2021) is reported the *Figure 2.4*, showing the trend of experimental data for bentonite, coming from different research, a clear dependence can be highlighted between swelling pressure and dry density. This trend confirms the necessity of design concepts to define a target dry density that will ensure a certain swelling pressure to develop within the tunnel.

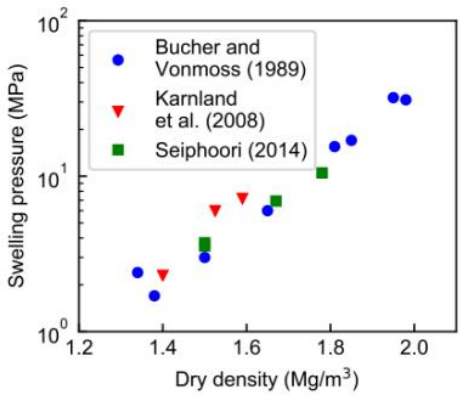

Figure 2.4 – Evolution of swelling pressure with dry density (Source: Bosch, 2021)

2.3 In Situ Full Scale Tests

Since the growing interest in deep geological repositories as a solution for nuclear waste disposal, it became fundamental the need of performing not only micro-scale test on materials involved but also full scale.

The motive behind full scale testing, other than assessing dimensions and feasibility of the setup, was to allow the investigation of “long-term” conditions and obtain experimental data to back calculate and calibrate numerical models for predictions.

2.3.1 FEBEX test

The FEFEX test project begun in the 1997 and nowadays it represents the longest full-scale project ever realised, with an acquisition data duration of eighteen years. In this project the Spanish Nuclear Waste Disposal concepts were used for the design of setup and materials. The underground laboratory operated by NAGRA in Grimsel (Switzerland), has been selected for the execution of the "in situ" test, in *Figure 2.5* is reported a picture of the site whilst in *Figure 2.6* an illustration of the bentonite blocks disposition is illustrated.

The purpose of the Full-scale Engineered Barrier Experiment (FEBEX) was to increase knowledge about the near-field of a repository for high level radioactive waste.

Let’s analyse the different phases that were passed through the project duration. Firstly, in 1997, after the completion of the tunnel excavation, two steel canisters with electric heaters were installed horizontally in the rock. The space between the canister and the host rock formation was filled with compacted bentonite blocks. Once the first phase was completed, the second phase was data acquisition, this lasted for over five years, before the first partial dismantling took place.

The purpose of the first dismantling was to build a model able to predict what the second dismantling would have shown. What was found in 2002, as a result of the environmental conditions to which bentonite was exposed, was that a dry density redistribution had occurred; since information coming from this first dismantling were used to calibrate

models and to predict the evolution of the phenomena, what was expected was a homogenisation trend of the dry density over time. With the second and final dismantling this trend was proven wrong because similar dry density values were found, showing that this process at some point had stopped and that no final homogenisation was been reached. (Bosch, 2021)

Figure 2.5 – the FEBEX at the Grimsel Test Site, Switzerland (photo taken from Kalinowski, 1997)

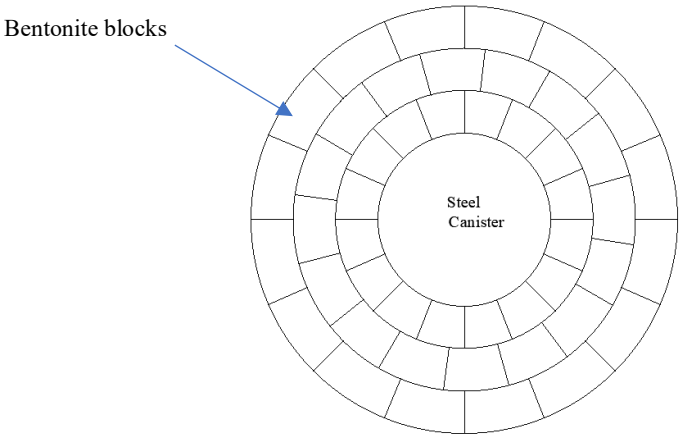

Figure 2.6 – Geometry of steel canister and bentonite blocks emplacement

The conclusions found after 18 years of data acquisition and the subsequent dismantling can be summarized in the following points:

- All the gaps between the blocks were found sealed, the granite/bentonite contact was tight, no preferential paths created

- The water content and dry density had an inverse trend, following a radial distribution was found that water content was decreasing, moving towards the centre of the tunnel whilst dry density was increasing, moving in the same direction.

2.3.2 Mont-Terri Experiment

For the Swiss concept, a full-scale experiment has been conducted in Mont-Terri underground laboratory, located in St.Ursanne, Switzerland.

The purpose was to assess fundamental behaviour aspects, associated with the short-term behaviour and long-term behaviour of the material in close vicinity to a drift, and factors that influence the development of an excavation damage zone (EDZ), concept that has already been exposed.

The Mont-Terri Rock Laboratory is situated in a 3900 m long motorway tunnel, in the Jura mountains of northwestern Switzerland, where at the laboratory depth the main geological formation is the Opalinius clay. Construction of the tunnel started in 1989 with the excavation of the main tunnel, within which the Rock Laboratory is situated. The Mont-Terri Project is leaded and monitored by the Swiss Geological Survey, on behalf of the Canton du Jura (Pearson & Schweiz, 2003).

In *Figure 2.7* is reported the configuration and extension of the galleries compounding Mont-Terri site. In the experiment the gallery was equipped with three heaters, supported by bentonite compacted blocks. the remaining gaps were filled by granular bentonite, according to the Swiss concept. The buffer is composed by highly compacted grains having a grain size distribution maximizing dry density.

The Mont-Terri experiment focuses more on the study of the host rock formation, OPA, indeed many fundamental findings have been done thanks to this project, a synthesis of

some of the main outputs was extracted from the Commemorative Publication written by Bossart (2021) on the official Mont-Terri project website, reporting the following:

- OPA exhibit extensive retention potential for radionuclides due to the large surface areas of clay minerals

- The processes through which radionuclides happens to be transported inside OPA is molecular diffusion, which is a rather slow process and concerns only weakly-absorbing radionuclides

- Some self-healing properties has been found and related to the smectite-illite content

- Heating generated by nuclear waste decay could create in the OPA formation a thermally induced damaged zone that would lead to reduction of sorption capacity

- The mechanical normal issues related to tunnelling construction at great depths such as EDZ and great tunnel convergence due to overburden

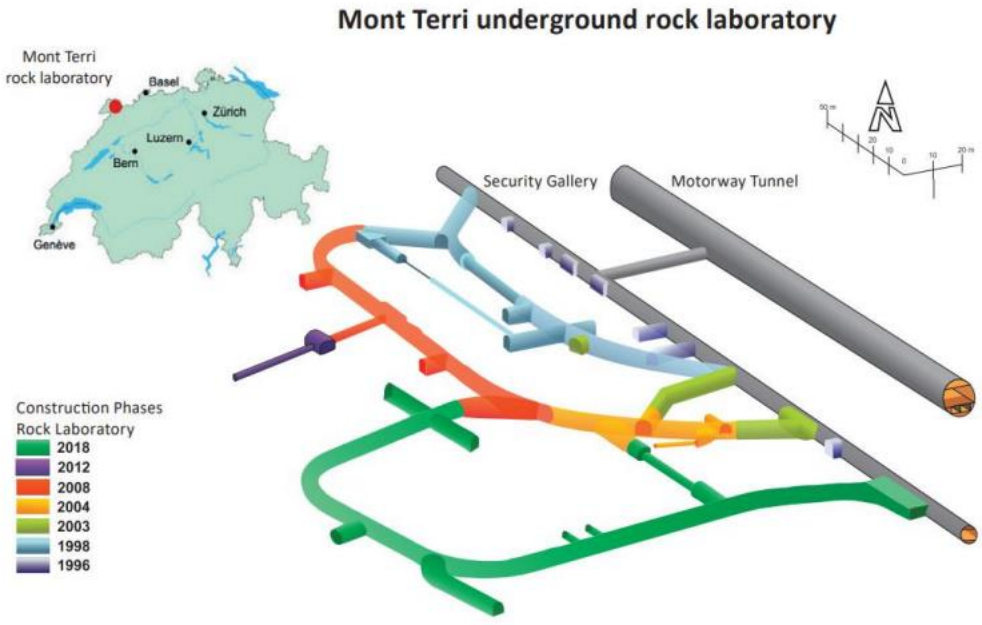

Figure 2.7 – Location and extension of Mont Terri underground rock laboratory (Source: Official site of Mont-Terri experiment)

3. Suction Concept and Mechanical Influence

In bentonites the hydraulic conditions play a huge role in governing the behaviour and the strength characteristics. During emplacement, both compacted blocks and granular backfilling will be in dry conditions, but as previously explained, the long-term scenario shows at least partial saturation of both fabrics. Therefore, it is of fundamental relevance a clear understanding of the mechanisms that theorize the bases of the so-called mechanics of unsaturated geomaterials, leading then to the possibility of applying these concepts to bentonite hydration and the consequential hydraulic properties.

The unsaturated field in soil mechanics is now at the centre of many different research projects worldwide; nonetheless as afore mentioned bentonite is a rather complex material, where the behaviour appears not to be consistent with some of the axioms that are nowadays considered to hold true in this developing field.

3.1 Water Retention Behaviour

To investigate the hydraulic properties of a soil, it's necessary to firstly introduce the concept of water retention behaviour. The water retention behaviour of a soil is explained by the relationship between the amount of water in the soil, defined either in terms of degree of saturation Sr or in terms of water content w; and negative water pressure for the capillary system, as shown in *Figure 3.1* below.

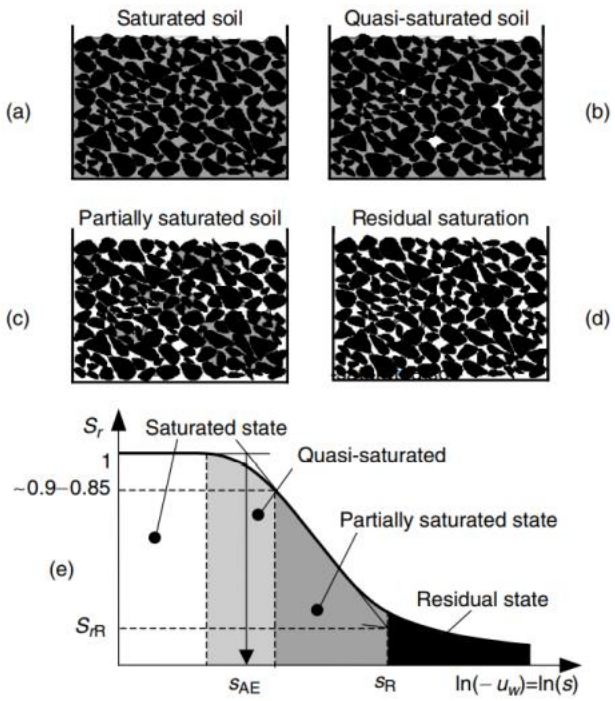

Figure 3.1 – States of saturation (Source: Mechanics of Unsaturated Geomaterials, L.Laloui, 2010)

In this curve it's possible to identify the different stages of saturation of a soil; if we imagine to study a REV (Representative Elementary Volume) of soil, from fully saturated conditions to dry conditions, through evaporation, it will pass through four main stages:

- Saturated state: there is the presence of a negative pressure, but the degree of saturation is still equal to 1;
- Quasi-saturated state: as evaporation proceeds, the negative pressure will bring to an increase of curvature, that will cause the expansion of air cavities in the larger pores within the soil and the degree of saturation will therefore decrease; air phase is still very discontinuous;
- Partially saturated state: in this phase the menisci reach the maximum curvature and air will enter the soil, the specific value at which this happens is known as *air entry value* and is a very important parameter that can be graphically identified in the curve; here air and water will be both continuous;
- Residual state: it's the final phase in which water is no longer continuous

The one just analysed is the behaviour of a soil going through evaporation, so from a saturated state to a dry state. The very same soil will not follow the same path in the reverse process. This is due to the nonlinear relationship between degree of saturation and suction.

The relationship it's indeed hysteretic, therefore for every soil is possible to define the water retention behaviour through two curves, the main drying and the main wetting, those curves mark the domain of possible attainable states for the soil and are therefore a unique characteristic of every soil. The area between the main wetting and main drying curves is the domain of hysteresis.

When moving between intermediate states, the soil will follow the so-called scanning curves, which unlike the main wetting/main drying, are reversible, and are represented in *Figure 3.2*.

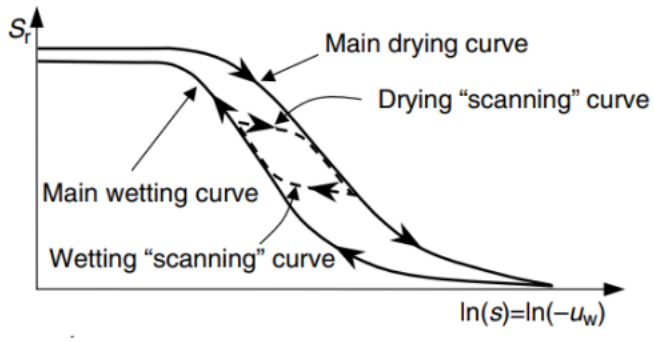

Figure 3.2 – Main Drying and Main Wetting with associated scanning curves (Source: Mechanics of Unsaturated Geomaterials, L.Laloui, 2010)

3.2 Suction

Total suction can be defined as the negative pressure that it is needed to be applied to the liquid water present in the measurement system in order to establish equilibrium through the vapor phase (Tarantino, 2010). It can be also defined as the potential energy per unit volume of water in the sample; the total water potential of a sample is the sum of 3 components:

• Gravitational: this potential depends on the position of water in a gravitational field

• Matric: this potential depends on the adsorptive forces binding water to the matrix

• Osmotic: this potential depends on the concentration of dissolved substance in the water

If now the REV analysed is just composed by water in liquid and vapor phase, water equilibrium will be obtained when the chemical potential of water in the liquid phase will be equal to the chemical potential of water in the gas phase:

$$u_w = u_v \tag{3.1}$$

Assuming a closed system formed by two layers in equilibrium, the first composed by vapour at p_v and air at p_a, and the second by simple water p_w. Imagine now to bring it to a state of liquid under negative pressure; we will have:

$$\int_0^1 d\mu_w = \int_0^1 d\mu_v \tag{3.2}$$

It is now introduced the chemical potential:

$$\mu = h - Ts = u + pv - Ts \tag{3.3}$$

Where:

- h is the enthalpy

- u the molar internal energy

- p the pressure

- v the molar volume

- T the temperature

- s the molar entropy

Subsequently it is introduced the first and second principle of thermodynamics, with the additional hypothesis that the work performed on the system is only caused by expansion work:

First principle: $$du = \delta q - pdv \quad (3.4)$$

Second principle: $$\delta q = Tds \quad (3.5)$$

Now substituting those equations in the preview's equation (3.3), we will find:

$$d\mu = vdp - sdT \quad (3.6)$$

Now, under the assumptions that water vapor follows the ideal gas law and adding the hypothesis of dT=0 (isothermal transformation), we obtain:

$$\int_0^1 v_w dp_w \int_0^1 \frac{RT}{p_v} dp_v \quad (3.7)$$

If the system is closed, the amount of molar volume of liquid water will be constant, so integrating equation (3.7), and explicating for pv:

$$p_v = p_v^0 exp\left[\frac{v_w(p_w - p_w^0)}{RT}\right] \quad (3.8)$$

Equation (3.8) shows how the pressure of vapour reduces as the pressure of the liquid decreases.

The water potential of a solid or liquid sample can be found by relating the water potential reading of the sample to the vapor pressure of air in equilibrium with it. So, it can be quantified by measuring the pressure that it is needed to be applied to water to establish equilibrium through liquid and vapor phase.

By inverting equation (3.8) is possible to derive total suction value as a function of a measurable quantity, being the water vapor pressure in equilibrium with the soil water, obtaining what is called psychrometric law (Thomson, 1871):

$$\psi = -\rho_w \frac{RT}{M_w} ln \frac{p}{p_0} \tag{3.9}$$

Where R is the universal gas constant (i.e., 8. 3143 J/mol K), ρ_w is the density of water, Mw is the molecular mass of water and T is the absolute temperature of the specimen and p/p_0 is the relative humidity RH.

In unsaturated soil, the concept of suction is rather complex and most of all not only related to capillarity.

For example, if we refer to clayey soils, as before said the concentration of cations is higher between two clay particles if compared with that in the solution, because of the negatively charged surfaces of clays particles. Because of this difference, water molecules chose as preferential path the one in between the two particles as an attempt to equalize the cations concentration. This very mechanism is known as osmotic mechanism and it's indeed common in clays geomaterials (Tarantino, 2010).

From literature is known that capillary mechanisms play a larger role when the suction in the soil is high, whilst they become irrelevant when the suction is low in spite of osmotic mechanism.

3.2.1 Suction Control

In the last decade it has become well known that suction plays a fundamental role in soils behaviour, being a parameter that affects strength characteristics of materials. Hence is important to reproduce certain ranges of suction on a lab scale, and to build SWRC to fully characterize a soil.

Despite several techniques exist to impose suction, it can be freely chosen one technique over another, since literature studies have shown that the mechanical properties are not affected by the technique used to condition the soil to a certain suction level.

In this chapter the illustrated technique is the one that will be forward used in the experimental campaign, that is Vapor Transfer technique. Vapor transfer/equilibrium techniques can be of two types; in the first type the control is exercised over the relative

humidity or total suction, in the second type the process is governed by a liquid phase transfer thanks to a salt-permeable interface allowing to control matric suction.

The first of the two is implemented as said by controlling the relative humidity of a sealed closed system from a vapor point of view, where the mass in keep constant. Therefore, soil water potential will be applied by means of water molecules migration through the vapor phase, the passage will happen from a reference system of known (imposed) potential to the soil pores, the process stops when equilibrium is reached (Romero, 2001).

The water potential of a solid/liquid is related to the vapor pressure of air in equilibrium with the sample, through the following law:

$$\psi = -\frac{\rho_w RT}{M_w} \ln (RH) \tag{3.10}$$

Where:

- M_w is the molecular mass of water
- p is the vapor pressure of the air
- p_0 is the saturation vapor pressure

The minus is needed since what the WP4C allows to evaluate is the water potential, being opposite in value to suction.

The way we impose the relative humidity inside the closed system is based on the various suction values that it's possible to obtain thanks to saline saturated solution, a variety of molecules allow to reach basically every suction level in a range between 386MPa<s<4MPa. More in detail, in Romero (2001) a table, reported in *Figure 3.3*, shows reports all the different compounds and the relative suctions attainable, with respect to temperature and solubility in H2O. Here, solubility will be the concentration of the compound necessary to gain the most stable crystalline phase, that will be in equilibrium with respect to the specified temperature.

Compound	T (°C)	A (%)	B (K)	u_v/u_{vo}(%) a 25 °C	ψ (MPa) a 25 °C	Solubility (g/100 g H_2O) 30 °C
$NaOH·H_2O$	15-60	5.48	27	6	386	113
$LiBr·2H_2O$	10-30	0.23	996	6	386	193
$ZnBr_2·2H_2O$	5-30	1.69	455	8	347	529
$KOH·2H_2O$	5-30	0.014	1924	9	330	128
$LiCl·H_2O$	20-65	14.53	-75	11	303	86
$CaBr_2·6H_2O$	11-22	0.17	1360	16	251	170*
$LiI·3H_2O$	15-65	0.15	1424	18	235	170
$CaCl_2·6H_2O$	15-25	0.11	1653	29	170	97*
$MgCl_2·6H_2O$	5-45	29.26	34	33	152	57*
$NaI·2H_2O$	5-45	3.62	702	38	133	192
$K_2CO_3·2H_2O$	20			44	112	113
$Ca(NO_3)_2·4H_2O$	10-30	1.89	981	51	92	156
$Mg(NO_3)_2·6H_2O$	5-35	25.28	220	53	87	74*
$NaBr·2H_2O$	0-35	20.49	308	58	75	98
$NaNO_2$	20			66	57	88
KI	5-30	29.35	254	69	51	153
$SrCl_2·6H_2O$	5-30	31.58	241	71	47	57*
$NaNO_3$	10-40	26.94	302	74	41	95
NaCl	10-40	69.20	25	75	39	36
NH_4Cl	10-40	35.67	235	79	32	41
KBr	5-25	40.98	203	81	29	71
$(NH_4)_2SO_4$	10-40	62.06	79	81	29	78
KCl	5-25	49.38	159	84	24	37
$Sr(NO_3)_2·4H_2O$	5-25	28.34	328	85	22	89
$BaCl_2·2H_2O$	5-25	69.99	75	90	14	38
$ZnSO_4·7H_2O$	20			91	13	62*
CsI	5-25	70.77	75	91	13	95
KNO_3	0-50	43.22	225	92	11	46
$CuSO_4·5H_2O$	20			97	4	24*
K_2SO_4	10-50	86.75	34	97	4	13

* solubility values possibly affected by solid phase changes, usually from one hydrated phase to another or from a hydrate to the anhydrous solid

Figure 3.3 – Saturated saline properties and solubility (Source: Romero, 2001)

The two parameters, A and B, reported in the above table, allow the evaluation of relative humidity changes with temperature for each of the compound reported, according to an empirical formulation that can be found in the paper.

The target suction is achieved positioning the sample to be treated in a desiccator with the solution of known concentration, under constant temperature.

The main flaw of this method is the time required to obtain equilibrium between pore water of the soil and surrounding solution.

3.2.2 Suction Evaluation

Independently from the suction control technique that one can choose to adopt to impose suction, it is necessary to use a procedure to check if the wanted suction is reached within the material; for this purpose, nowadays the most easy and fast device capable of measuring water potential is the WP4 dew point potentiometer.

This instrument, that is reported in *Figure 3.4*, allows the measure of water potential (opposite of total suction) of a soil specimen, positioned into a rigid round cell, made of brass with a diameter of 30mm, called Microcell.

Figure 3.4 – WP4C device (Source: Ferrari et al., 2014)

The WP4C measures the sum of the osmotic and matric potentials in a sample, without giving the possibility of knowing each contribution. Often one or the other of these potentials will be the dominant factor in determining the total potential. The measure is given by equilibrating the liquid phase water of the sample with the vapor phase water in the headspace of a closed chamber, then measuring the vapor pressure of the headspace.

The dew-point chilled-mirror psychrometer functioning can be explained thanks to components reported in *Figure 3.5*, it is based on the presence of a mirror inside the sealed chamber, with a precisely controlled temperature. The specimen inside it controls the relative humidity, and a fan allows the environment to reach equilibrium. That way the temperature of the mirror is progressively lowered, and a photoelectric cell captures the exact moment condensation occurs in the mirror. The corresponding temperature of the

specimen is measured. Once the relative humidity is measured by the device, the total suction is obtained using the psychrometric law.

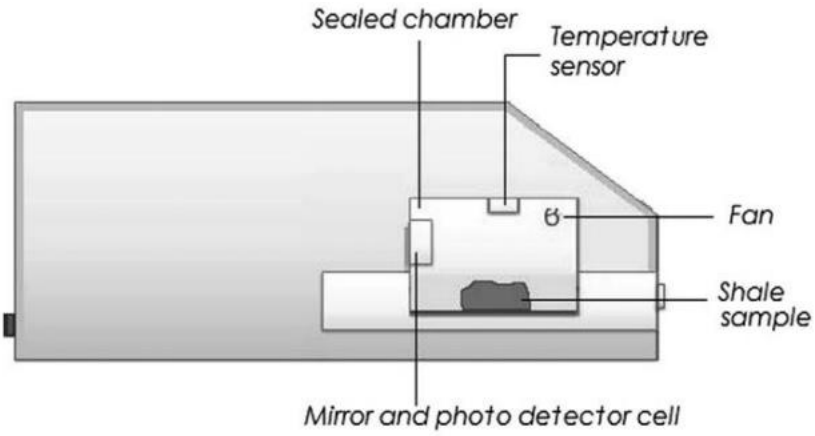

Figure 3.5 –Inside components of WP4 (Source: Ferrari et al., 2014)

The accuracy of the device as specified by the manufacturer is ±0.05 MPa for total suction from 0 to 5 MPa and 1% for total suction in the range of 5–300 MPa.

3.3 Effective Stresses in Unsaturated Field

The effective stresses are a combination of both the externally applied stresses and the internal pressures of fluid phase and the concept introduced enables the conversion of a multiphase porous medium, into mechanically equivalent single-phase continuum.

Since Terzaghi's effective stress is valid only for the limit states of full saturation of pores with one fluid, it was necessary to extend the effective stress principle to unsaturated states, to account for fluids of different natures.

To introduce the concept of effective stress, it is necessary that the defined stress variable meet the following requirements:

- Elasticity and elasto-plasticity: $\varepsilon ij = Cij * \sigma' ij$
- Simplification: the effective stress variable should lead to a simplification of experimental data interpretation

- Applicability: when defining the effective stress, the variables introduced need to be measurable

An effective stress-based modelling approach requires conceptually converting a generic multiphase medium into a single mechanically equivalent continuum medium (Nuth & Laloui, 2007). As before said, the presence of clay minerals brings significant interactions between solid mixture and water molecules, the more active and expansive the clay minerals are, the more these mechanisms amplify.

A milestone in the effective stress formulation in the unsaturated field was given by Bishop (1959), where the author defined the effective stress as a function total stress and pore pressure, through an extension of Terzaghi's formulation for saturated soils, therefore defining the effective stress as: "The excess of the total stress over an equivalent pore pressure" (Nuth & Laloui, 2007). The obtained formulation is:

$$\sigma'_{ij} = \left(\sigma_{ij} - u_a\delta_{ij}\right) + \chi(u_a - u_w)\delta_{ij} \tag{3.11}$$

Where:

- χ is the Bishop's parameter
- σ_{ij} is the net stress
- $(u_a - u_w)$ is the matric suction
- δ_{ij} is the Kronecher delta

From equation (3.11) it is possible also to highlight that for fully saturated conditions, Terzaghi's formulation is restored.

The Kronecker delta allows for the transformation of the matric suction into a tensor, specifically:

$$\delta_{ij} = \begin{cases} 1 \; if \; i = j \\ 0 \; if \; i \neq j \end{cases}$$

Back to equation (3.11), the first term represents the net stress whilst the second one the matric suction. This formulation aims at averaging the stresses over a representative

elementary volume containing all constituents: air, water and solid grains. If the Bishop parameter is equal to zero, one recovers Terzaghi's expression for the saturated case, this very parameter was introduced as a scaling factor for matric suction.

Reformulating the above equation, one obtains:

$$\sigma'_{ij} = \sigma_{net-ij} + \chi s \delta_{ij} \tag{3.12}$$

Bishop and Donald (1961) first attempt to verify Bishop's relation experimentally was to consider:

$$\chi = \chi\,(Sr) \tag{3.13}$$

Where S_r is the degree of saturation and the effective stress is assumed to be valid within the elastic domain.

Known the complexity of the problem, the modelling should be based at least on two constitutive stress variables (Gens, 2010):

- Mechanical stress variables, being any stress variable that can be used to describe the either elastic or elastoplastic evolution of strains for the solid skeleton
- Hydraulic stress variables, being any stress variable that can be used to describe the pore water pressure evolution

So, a modified version of Bishop's effective stress is implemented by Jommi and Di Prisco (1994) where the second stress variable is added to complete the description of the hydraulic behaviour:

$$\sigma' = \sigma_{net} + S_r * s \tag{3.14}$$

Therefore, to describe the mechanical behaviour of the soil, the Soil Water Retention Curve has to be evaluated.

Among the many effective stress's approaches based on the same concepts as the one reported above, another modification of Bishop's effective stresses made by Lu et al. (2010) is in the following explained. The approach used by the authors is based on the introduction of an effective degree of saturation, function of a residual degree of saturation. To understand the reasons behind the need to introduce this variable, by the authors is explained that for very high suction levels a thin film of water is surrounding the particles, indeed the residual water content deriving from this film is supposed to have an influence of the effective stress.

The modified formulation is reported in the following:

$$\sigma'_{ij} = \sigma'_{ij,net} + S_{r,e} s_m \delta_{ij} \tag{3.15}$$

Where:

- $\sigma'_{ij,net}$ is the net stress tensor
- s_m is the matric suction
- $S_{r,e}$ is the effective degree of saturation, which according to the proposed approach in equal to:

$$S_{r,e} = \frac{S_r - S_{r,res}}{1 - S_{r,res}} \tag{3.16}$$

Where Sr,res represents the residual degree of saturation, which in the s-Sr plane represents the tale of the curve.

The last formulation reported was developed by Tuttolomondo (2021) for active clays. In the author's studies the contribution of pore water chemistry and the interactions between clay mineral and water was considered as a scaling factor for the suction contribution. In the following the relationship is reported and each term is furtherly discussed:

$$\sigma'_{ij} = \sigma_{net-ij} + S_r(s_m - s_{s,e})\delta_{ij} \tag{3.17}$$

Where:

- σ_{net} is the net normal stress;

- S_r is the degree of saturation
- s_m is the matric suction
- $s_{s,e}$ is the effective solute suction
- δ_{ij} is the Kronecher delta

The effective solute suction is defined by the author as the difference between the solute suction of the pore water, $s_{s,pw}$, and the osmotic suction of the water:

$$s_{s,e} = s_{s,pw} - s_s \tag{3.18}$$

This factor is related to the presence of the before defined movable and non-movable ions in the diffusive layer, where $s_{s,e} = 0$ means that no non-movable ions are detected, in particular for such case the Bishop's effective stresses formulation is restored.

The above exposed formulation is designed to give a unique ultimate failure envelope irrespective to the chemical composition of water within the pores of the soil.

4. Experimental Techniques for Suction Control

This part is dedicated to the explanation of the experimental techniques and the attempts done to achieve suction control, based on the theory exposed in the previous chapter. Specifically, whilst according to theory, the vapor equilibrium technique is very simple to be adopted to impose suction to a soil sample, from a practical point of view, the realization it's very delicate but most of all, time-consuming.

The objective was to impose two different suction levels to the soil, needed for further shear testing under certain environmental controlled conditions. The levels were:

1. s= 40 MPa
2. s= 15 MPa

The two arbitrary suction levels chosen were meant to be representative of different saturation states of the soil, if imagined in the WRC where the suction values are reported in logarithmic scale.

4.1 Properties of Tested Material

The starting point of the material to condition was hygroscopic lab conditions, hence the initial suction value was in the range of 127-135MPa, with a water content of around 6%.

The material tested is a Bentonite MX80, mix.2. It is a sodium-based bentonite and the initial characteristics are reported in *Table 4.1*.

Smectite Content	***Cation Exchange Capacity CEC***	***Liquid limit w_l [%]***	***Water Content w [%]***	***Plastic limit w_p [%]***	***Bulk Initial Density ρd [g/cm³]***	***Void Ratio e_0 [-]***	***Specific Gravity Gs [-]***
84.9%	72.16	≈ 420	≈6	≈65	1.36	0.75	2.74

Table 4.1 – Initial Bentonite Conditions

4.1.1 Sample Preparation

To prepare the material, information about the granulometric distribution were gained from a past study conducted at EPFL, among the reported different grain size distributions it was chosen to use the *Fuller-type* grain size distribution; meaning that all the different grain sizes will be comprised inside the sample.

Therefore, in *Figure 4.1* is reported the Grain Size Distribution (GSD) that will be adopted for further testing.

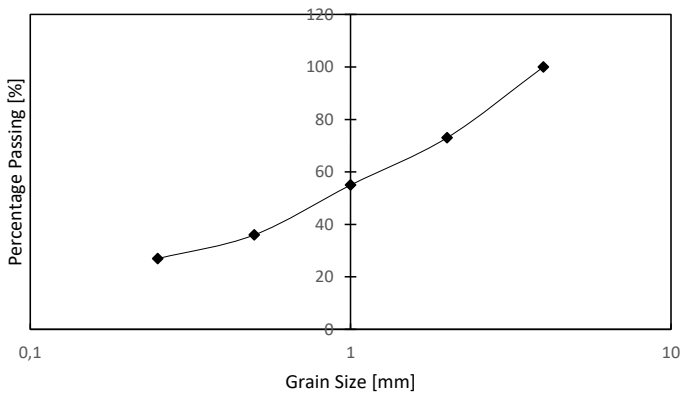

Figure 4.1 – Fuller- type GDS used

The amount of material to be prepared is a function of the number of samples and tests that will be performed. It's important to understand that when conducting an experimental campaign many variables need to be analysed before finding the right procedure and for this very reason it's always useful to have more material than the one considered strictly necessary.

In *Figure 4.2* are reported the sieved granulometries, needed to assemble the correct granulometry of the fabric to be tested. The initial mixture was sieved into five ranges, each range of the soil sample is considered to be uniform.

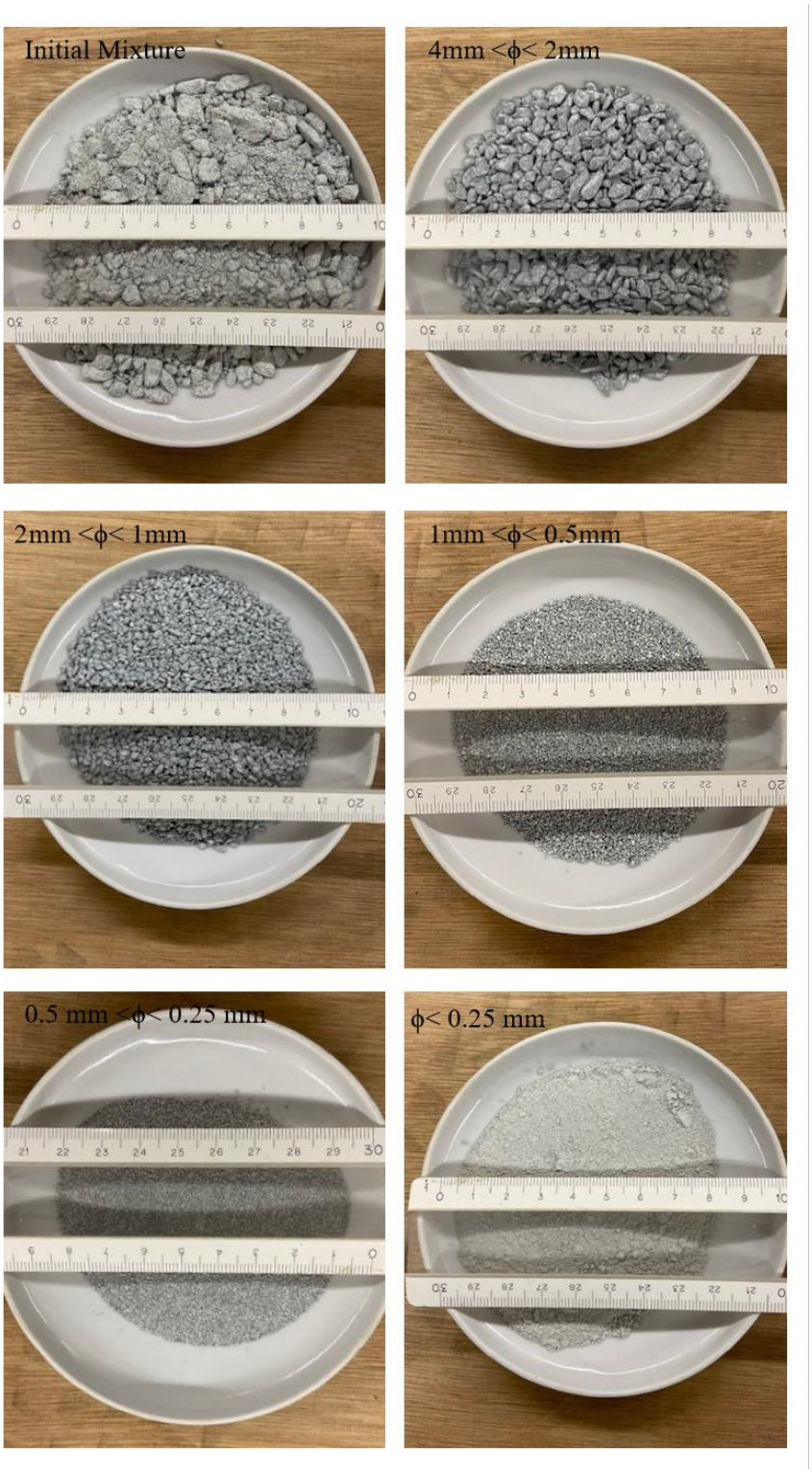

Figure 4.2 – Bentonite in all his grain sizes

From the grain size distribution, it was possible to acknowledge the percentages of each granulometric fraction, as reported in *Table 4.2*.

Fraction [mm]	*Percentage passing [%]*	*Percentage hold [%]*
4	100%	0%
2	73%	27%
1	55%	45%
0,5	36%	64%
0,25	27%	73%

Table 4.2 – Percentage of passing and hold material

4.2 Vapor Equilibrium Technique

4.2.1 Saturated Saline Solution

As previously described, vapor equilibrium technique allows to impose a certain suction value to soil samples through vapor diffusion from saturated saline solutions to the soil.

Consulting the table from Romero (2001) two saline solutions were chosen to reach the suction levels wanted, NaCl and KNO_3, which were meant to ideally impose to the soil suction values of respectively 40 MPa and 10 MPa.

Two sealed jars were used, one for each saturated saline solution. Both saturated saline solutions were given the time to equalize and were then checked using WP4C, to validate the suction level according to what stated in *Figure 3.3*, reported in the previous chapter.

Then inside each of the two jars the samples were positioned, the jars were closed granting the sealing with the help of grease distributed equally over the edges of the cover.

The first protocol used was to check the evolution of the mass and suction daily for a time window of 30 days, the data obtained are linearly interpolated and reported in the graph in *Figure 4.3* below.

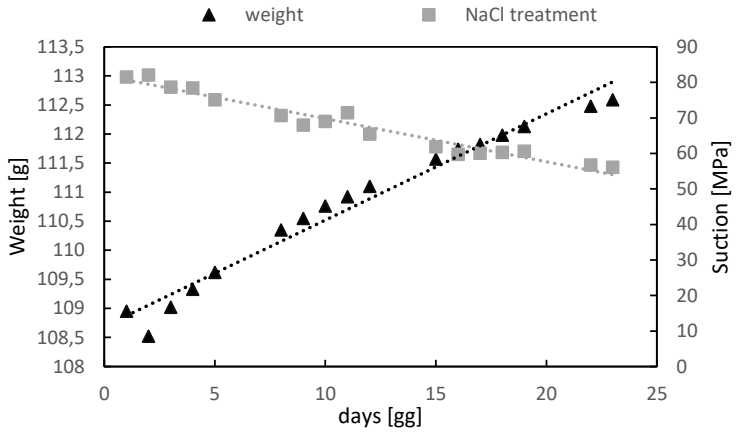

Figure 4.3 – Evolution of suction and weight value in 28 days

As it is possible to notice from the time evolution of the suction values for the sample of soil treated with the use of vapor equilibrium technique and the saturated saline solution NaCl it is a slow process. The target value imposed was, as said before, 40MPa, and after 30 days of conditioning the value obtained was around 55MPa, which meant that from the starting point the value decreased of around 30%.

Two reasons were found as an explanation:

- Disturb caused from the frequent checks;
- Leakage of the jars

It was decided to proceed dividing the soil inside the two initial jars in more smaller jars, like the ones reported in *Figure 4.4*. The idea behind the decision is that in a smaller environment it's easier to reach equalisation therefore to impose the wanted relative humidity. Also, the checking procedure became less frequent, knowing that very little changes of temperature or relative humidity can lead to very high changes of suction, as it is possible to notice just looking at the connections between these variables described by the psychrometric law.

Therefore, boundary conditions need to be taken carefully into account.

Figure 4.4 – Decreasing the chamber area with smaller jars usage

Even though reducing the chamber's area and soil quantity allowed to accelerate the process, it took anyway few months to get close to target, demonstrating that this technique it's not suitable when time it is a fundamental issue. Also, in parallel, since it was necessary to dispose of huge number of samples for the testing campaign, two bigger jars containing always the saturated saline solutions were used, each fitted 4 samples, as reported in *Figure 4.5*.

Figure 4.5 – Parallel usage of different jars

4.2.2 Demineralized Water

Since it was possible to notice the rather long period required to condition the samples through Vapor Equilibrium Technique if using saturated saline solutions to impose the target relative humidity; it was decided to endure with the vapor equilibrium technique, due to its undeniable simplicity, but with the imposition of the lowest suction value attainable, being ideally zero suction, through demineralized water.

As reported in *Figure 4.6* below, this attempt was pursued through the usage of the smaller jars, and suction values were evaluated once a week for a time period of 28 days.

Figure 4.6 – Demineralized Water Treatment

With the only purpose of understanding the limits of this technique related to the tested bentonite, in its as-pureed-state and in absence of any compaction, it was recorded that the lowest total suction value obtainable was of 4.77 MPa corresponding to a water content of 23.25%.

4.2.3 Water Adsorption through Vaporisation

Seeking for the fastest route to conditionate and equalize the samples to the target suction level, it was considered worthy to try to lower the suction value by increasing the water content.

Since an experimental water retention curve for the same bentonite (reported in *Figure 4.7)* – different granulometry – was known thanks to the past work done by Seiphoori (2014), the idea was to derive from the curve the amount of water mass to spray on the sample to achieve the target suction value.

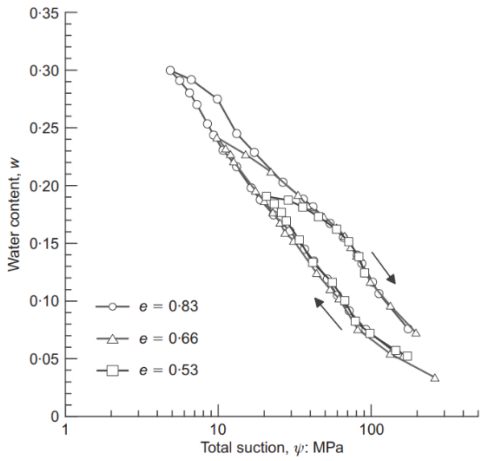

Figure 4.7 – WRC for bentonite MX80 (Source: Seiphoori, 2014)

In the following *Figure 4.8* a comparison between the bentonite fabric hydrated according to the two different techniques.

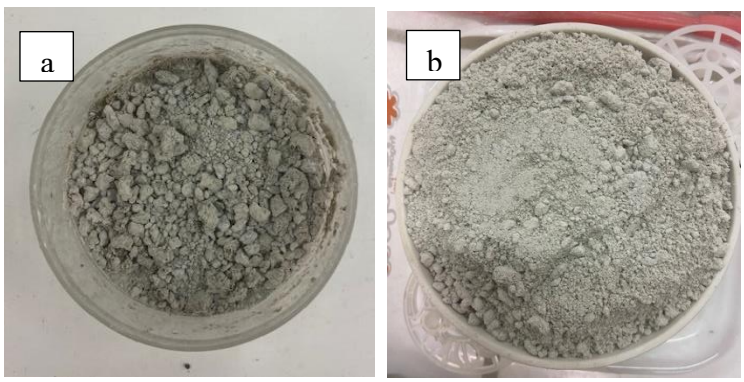

Figure 4.8 – (a) Sprayed sample; (b) Vapor equilibrium treated sample

It was already possible to perceive the differences in the two fabrics, in terms of "grain" dimensions; the sprayed sample showed the formation of lumps whilst the sample treated with vapor equilibrium looked considerably more swollen and "lumpless".

Another concern was the difficulty in assuring a real water content homogenization, perhaps the time needed for the process to conclude itself could represent a decisive factor; the use of this technique no longer represents an advantage.

To seek for mechanical validation of the difference seen at a macroscopic scale, the sample reported in Figure 4.9(a) was loaded to 1000 kPa and the mechanical response was compared to the one of a sample (b), treated with vapor equilibrium technique. The suction at which this comparison is done is ≈ 40 MPa, the results of the response upon compression obtained are reported in the following *Figure 4.9*.

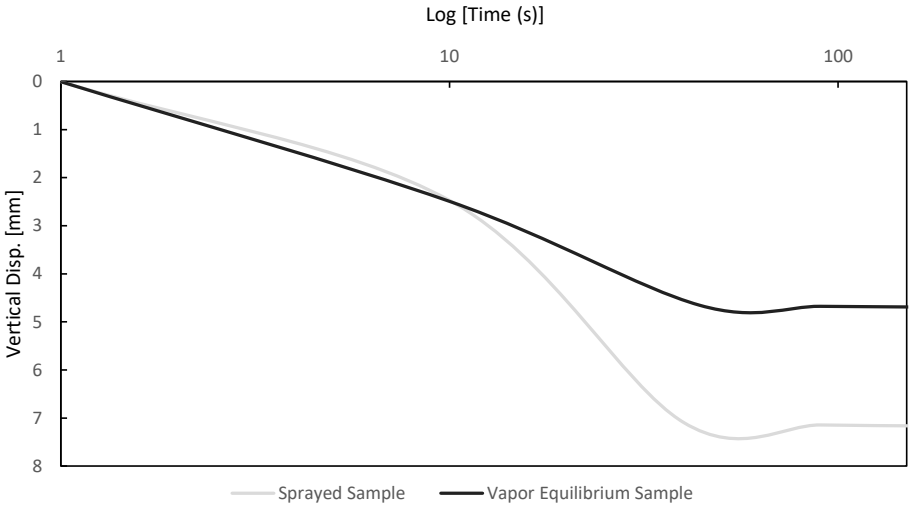

Figure 4.9 – Comparison in terms of the consolidation

It is possible to highlight that the response in terms of compression for the two samples is similar but leads to different values of final vertical displacement; in particular the sample whose suction was imposed spraying water over the surface had given higher values of vertical displacement under the same loading conditions.

Possible reasoning can be given imagining that in the sprayed sample the grains are attached to each other, creating sticky lumps. The water present can be associated to bulk water, that can be considered easier to loose than pore water (solid water). Along the test

duration it can be imagined that this amount of water filling the pores will evaporate leaving air filled pores, that will be compressed under the load application. If the vapor equilibrium technique is used, the pore water has a network of pores with in-tension membranes given by the menisci mechanism, allowing more resistance to compression.

Little validation can be found if known that actually higher decrease of water content was detected in the sprayed sample, after test duration, if compared with the loss of sample treated with Vapor Equilibrium Technique.

4.3 Adopted Protocol

Lastly it was possible to compare all the investigated strategies, in terms of suction evolution, to get to the final protocol to use for suction control. In the following *Figure 4.10* are reported the suction changes over a period of 28 days for the sample treated with demineralized water, interpolated according to a logarithmic curve.

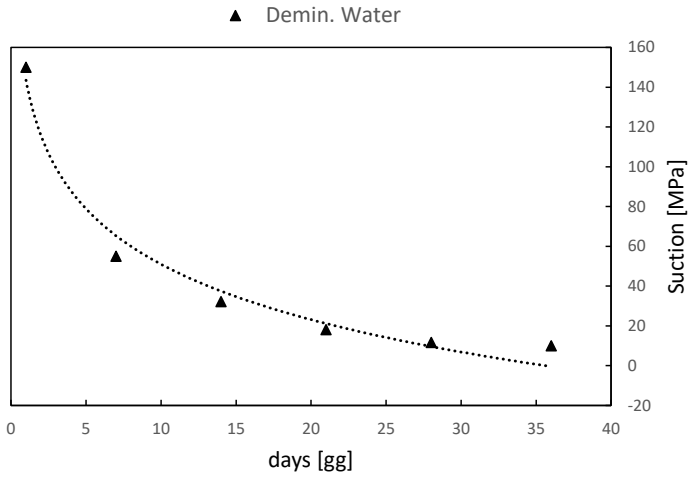

Figure 4.10– Suction evolution for sample treated with demineralized water

The above reported trend is compared with the one obtained for the sample treated with vapor equilibrium technique, for the NaCl saturated saline solution, as reported in *Figure 4.11*.

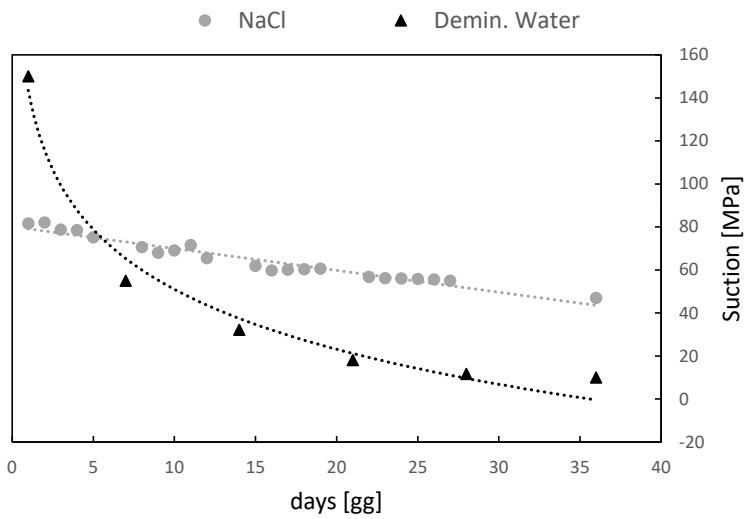

Figure 4.11 – Comparison between the suction evolution trend for the two solutions

The efficiency, in terms of rate of suction decrease, of the second method is unequivocally higher, leading to a final suction value (after 28 days) 89% lower than the initial.

The final protocol adopted was the result of many attempts, the purpose was to find a fast way of decreasing suction but without losing focus on the need of having a sample of soil stable with the saline solution that was then to be used during the shear test.

It was achieved combining the effects of demineralized water and saturated saline solution, clearly the time needed to reach the two suction's target was different. Specifically, according to what reported in the previous *Figure 4.12*, to achieve 40MPa the sample was firstly treated for one week with demineralized water, then moved to a secondary jar containing NaCl saturated saline solution 48 hours before any test was performed. To achieve 15MPa the same procedure was followed, but instead of one week, the preliminary conditioning in demineralized water lasted two weeks.

The meaning of the 48 hours was, as said before, to guarantee that the sample was in equilibrium with the target suction value, so that over the test duration was easier to state that the environment was not only sealed but also stable.

4.4 Water Retention Curve for Bentonite

Thanks to the set of data accumulated along the calibration process and also as a consequence of the subsequent experimental campaign conducted to evaluate shear strength, it was possible to obtain a water retention in terms of water content, as reported in *Figure 4.12*.

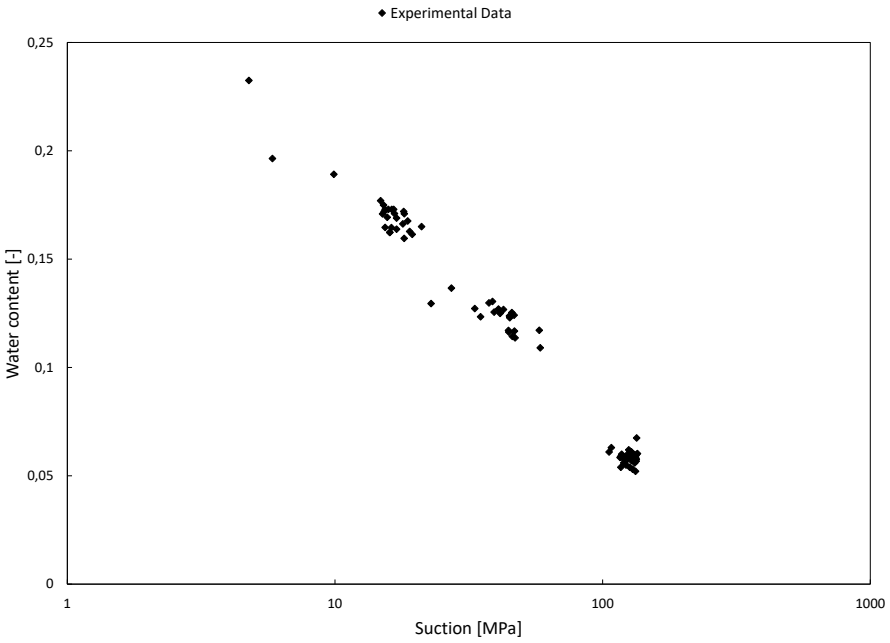

Figure 4.12 – Water Retention Curve

Since during the experimental work many decisions were guided following the past work of Seiphoori (2014) it felt of relevance to compare this very WRC with the one obtained by the author. The two set of data are reported below in *Figure 4.13*.

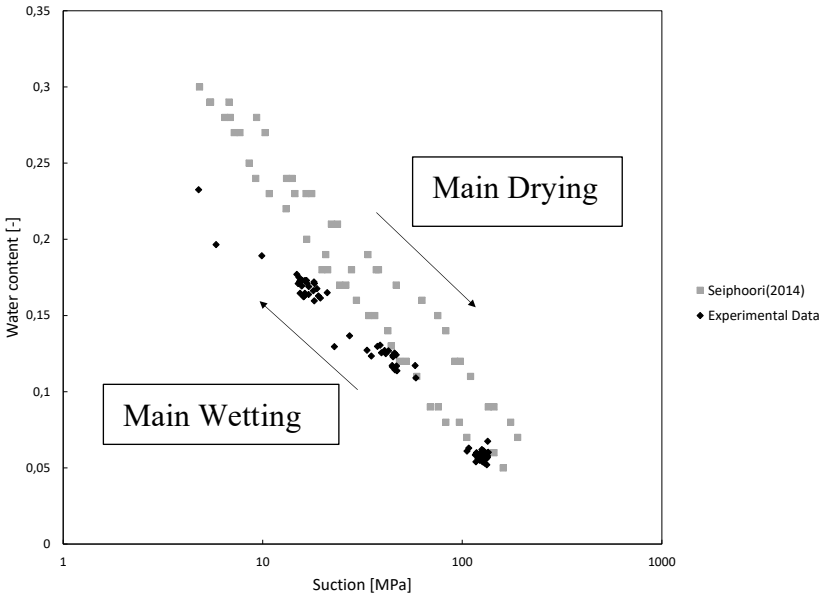

Figure 4.13– Experimental results compared with literature

In *Figure 4.13* are reported experimental results and Seiphoori's results, where the represented dots belong to the main drying and the main wetting path, however the data obtained in this campaign belong only to the main wetting.

It is possible to see how data obtained fit nicely with Seiphoori's ones for high suction values, whilst the two "trends" drift a bit apart for lower suction values. An interpretation to this behaviour can be given remembering that the GSD used in the two campaigns are different, specifically Seiphoori's grain size distribution defines even finer fractions.

Since no evaluation of the changes of void ratio within suction change was performed during the wetting process, it is not possible to express the WRC in terms of degree of saturation. That would have allowed the fitting of the curve thanks to Soil Water Retention Functions, like the one implemented by Van Genuchten back in 1986.

Therefore, the procedure used consists of trying to fit the experimental data with different mathematical formulations, searching for the one that best interpolates the data collected; simply trying in steps to interpolate data starting from a linear interpolation and increasing each time the complexity of the interpolating equation used.

Also, since the collected data of water content and suction mainly cover the range of interest investigated, it was rather difficult to interpolate what can be assimilated as three cluster of points.

To evaluate if the interpolating quality was increasing while changing the equations, a reference statistical parameter was taken, specifically the R square value. This statistic quantity it's an indication of the standard deviation between data obtained through the interpolating equation and experimental values.

Three different fitting equation are reported in the following *Figure 4.14*, with the associated used equations and R square value reported in *Table 4.3*.

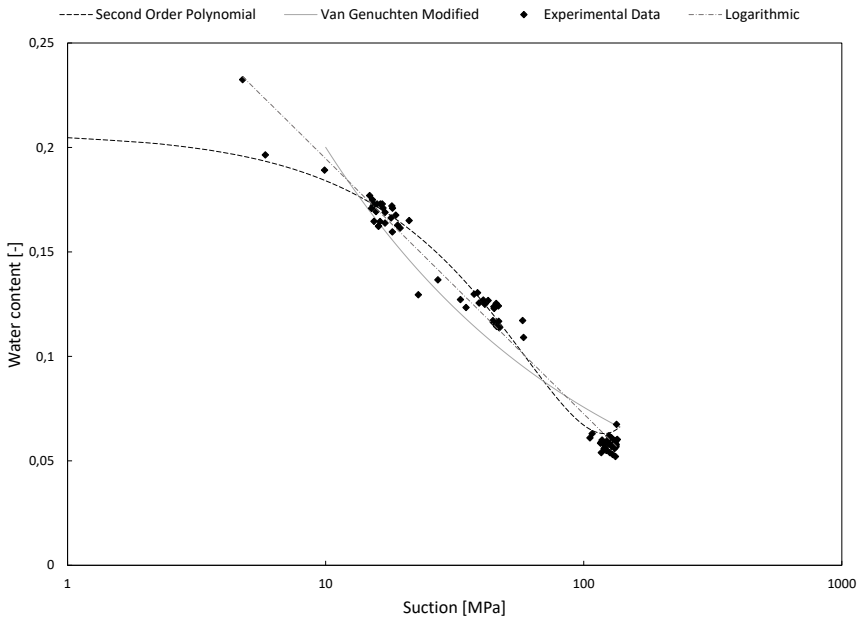

Figure 4.14 – Fitting trial of the soil water retention curve

Type	***R^2***
Logarithmic	0,9837
Second Order Polynomial	0,9825
Modified Van Genuchten	0,9134

Table 4.3 - R square values for each fitting

The equations used are reported in the following list:

- $y = 10^{-5}x^2 - 0{,}0024x + 0{,}2071$ (4.1)
- $y = -0{,}053\ln(x) + 0{,}3168$ (4.2)
- $y = \left(1 + \left(\frac{x}{0{,}22}\right)^{1{,}42}\right)^{\left(\frac{1}{1{,}42}-1\right)}$ (4.3)

Where the last equation is an adaptation of Van Genuchten (1986) formulation, where the degree of saturation was substituted with gravimetric water content.

One aspect that makes very difficult to use Water Retention Functions that were developed for clayey soils with bentonite clays is the peculiar absence of the final constant tale typical of WRC. Indeed, the known S shape of WRC doesn't apply to bentonite because of the high retention capacity, leading to a difficult to assess a residual water content, concurrently it is known that the soil can withstand very high levels of suction.

5. Experimental Campaign for Shear Strength Evaluation of Bentonite

For this part of the experimental campaign Tested Material and Sample Preparation are the same described in the previous chapter.

5.1 Direct Shear Test

Shear strength is defined as the maximum resistance that a material can withstand when subjected to shearing. To evaluate it the soil specimen is placed in an apparatus known as shear box which, in his standard configuration, consists of: two metallic plates, two porous stones, two screws, a gripper disk and a loading cap; over it the normal stress is applied by means of a loading piston in contact with a loading ball. The shear box restricts the specimen's horizontal strain but enables shearing on a horizontal plane where the two metallic plates meet. The shear box is then placed in the shearing device. Initially, a direct normal pressure is applied at the top of the sample using a leverage weight or via pneumatic system. This phase is known as the consolidation stage and proceeds in an incremental manner similarly to that of a typical consolidation test. At this stage, the metallic plates are screwed together.

Before the shearing stage begins, the two screws securing the upper and bottom parts of the shear box are removed, then the upper metallic plate is slightly raised by means of two screws, to ensure the separation of the two pieces of the apparatus and secure that the normal and shear loads are transmitted only through the specimen.

Afterwards, a shearing stress is applied along the pre-determined horizontal plane until the specimen fails or until a certain design horizontal displacement is reached. Hence, in the direct shear test the failure plane is imposed by the setup configuration, whilst in triaxial testing the failure occurs within the specimen, along the weakest plane.

The test is governed by a rate, more specifically the ratio between horizontal displacement and time, this very rate in linked to the soil characteristics and for clays should be relatively small to prevent pore pressure built up and also to allow the reorganization of

the grain distribution along the shearing surface. It is controlled by a servomotor device and a gear box assembly.

The vertical and horizontal deformation are calculated via dial gauges. Each displacement measurement was made by a Linear Variable Differential Transformer (LVDT) displacement transducer.

A schematic example of the components of the box is shown in *Figure 5.1*.

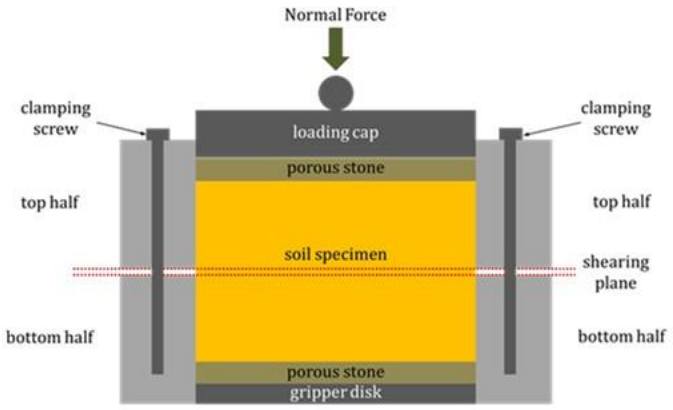

Figure 5.1 – illustration of direct shear components

5.1.1 Procedure

The whole campaign consists in performing shear tests for three different suction conditions, that are:

- Hygroscopic, s= 120-130 MPa
- Conditioned sample, s= 40 MPa
- Conditioned sample, s= 16 MPa

For each suction condition, as usual, a geometric succession of loads will be imposed. The six decided loads were 100, 200, 500, 1000, 1500 and 2000kPa. In *Figure 5.2* is reported a picture taken of the direct shear test device with the shear box docked and ready for shearing phase.

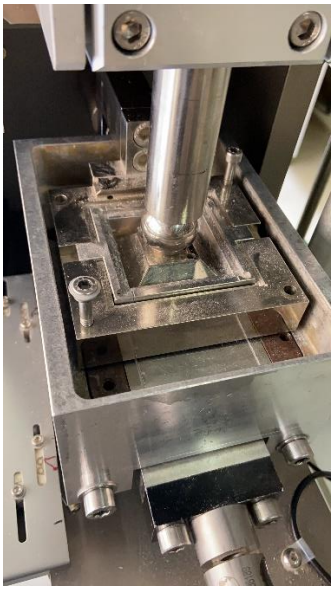

Figure 5.2 – Shear box docked to GDS and loaded

The preparation procedure can be summarized in the following stages:

1. The necessary amount of soil was weighted, starting from the knowledge of the volume of the shear box and the density of the material
2. Additional soil is taken to evaluate the water content, so it is weighted and positioned in the oven
3. Additional soil is taken to evaluate total suction, with WP4C device
4. The shear box is assembled using two screws to fix the upper and lower part
5. In the bottom of the shear box is positioned the steel gripper disk and over it is poured the specimen, assuring a horizontal surface before positioning the load cap
6. Then the shear box is positioned in the GDS machine, and it is docked thanks to two bigger screws that allow to fix the bottom part of the device, this part will be the one moving while shearing
7. The loading ball is positioned over the loading cap, the load will be transferred by the piston to the sample's surface homogeneously through it

At the end of each test point 2 and 3 are repeated to collect a dataset of information regarding beginning and end of the test, since it will be crucial, as furtherly discussed, to know the variation of these quantities in the time window of a test.

5.2 Preliminary Tests

In every experimental campaign it is essential to perform some preliminary tests to assess the best strategy and also the repeatability of the test itself.

Since the shearing characteristics (shear box dimension, rate etc) will be kept constant for the three different set of tests to be performed, the preliminary tests are performed for the hygroscopic samples, as is the easiest configuration.

To obtain valuable results, it is necessary to reduce to a minim errors or misinterpretation of data related to some variable that we can control. For this reason, couples of tests were performed changing one variable each time, the chosen variables are:

- Shear box dimension
- Shearing rate
- Shearing device

The consideration derived are reported as follows.

5.2.1 Shear box dimension

For this first variable, under the same load condition, which was 1000kPa, the same test was performed once with the 60x60 shear box and secondly with the 45x45 box. In *Figure 5.3* are reported the two resulting curves, in terms of horizontal stress-horizontal displacement, obtained after the test.

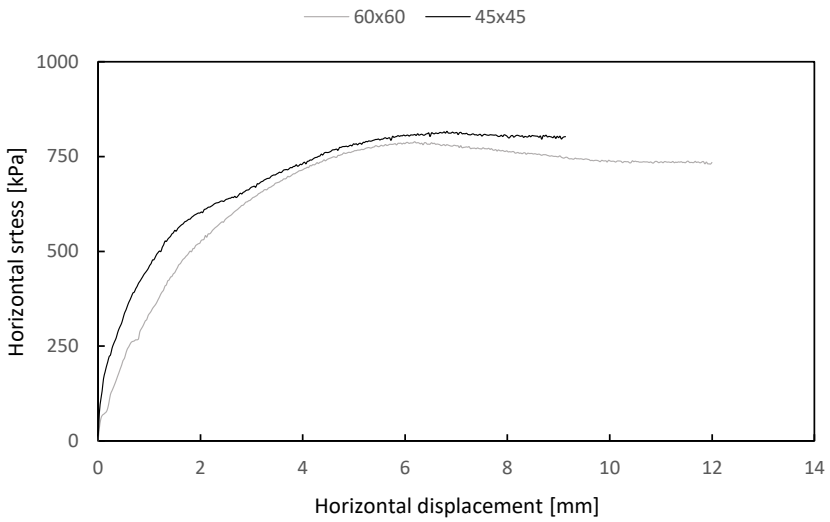

Figure 5.3 – Comparison between shearing response attained with two different box's dimensions

If we look at the shearing behaviour obtained, is possible to notice that the difference in terms of shear strength peak value, is around 25 kPa, which accounting the vertical load applied can be pointed out to be irrelevant.

Another difference that is shown is the shearing displacement, but this is related to the machine configuration, that with 45x45 box allows to have a shearing target displacement around 30% lower than the one that is possible to obtain with the 60x60, leading to a maximum horizontal displacement of 9mm.

5.2.2 Shearing Rate

The second variable analysed is the shearing rate, to understand the relevance the same test was performed this time for two different load conditions, being 1000kPa and 2000kPa, firstly with a shearing rate of 0.05mm/min and secondly with 0.1mm/min. In *Figure 5.4* are reported the four resulting curves, obtained after the tests, in terms of horizontal stress-horizontal displacement.

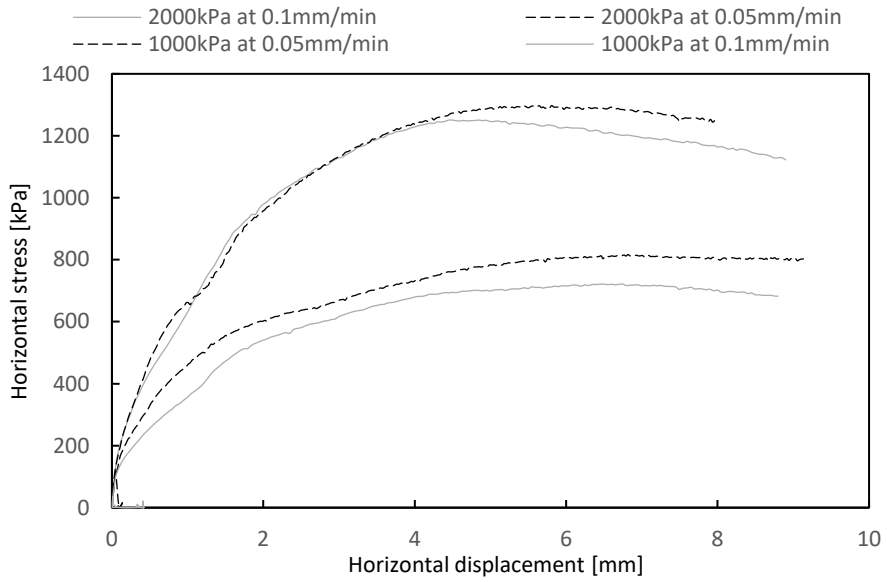

Figure 5.4 – Comparison between shearing response attained at two load level for two shearing rates

The conclusion that can be derived from this confrontation is that, as it was possible to imagine, no huge difference in shearing behaviour can be found in the 2000kPa, because the higher the load the less relevance shearing rate has, also grain crushing gets to lead more the response, thus is possible to say that the peak values will be more linked to that than to the time needed to reorganize the grain distribution during shearing.

Whilst for the 1000kPa tests, it's possible to notice that a lower shearing rate gives back a higher shear strength value, therefore using a faster rate leads to underestimation of peak shear strength.

Both shearing rates can be acknowledged into the range of fast rate if it is remembered that the soil tested is a clay, the reasoning behind these choices is the assumption that either way the tests will be in undrained conditions. Hence, the decision about the rate to use was guided by the need of avoiding major grain crushing.

During these trials one test was performed, for 1 MPa vertical load, stopping the shearing phase for 2 hours, then the test was restarted; the purpose was to seek for a "jump" in horizontal stresses value, that would have shown a too fast rate.

Indeed, if this behaviour would have been found, the "jump" would have meant that the soil, if given the time, would have reassessed his internal structure returning a higher resistance to the applied shearing force.

5.2.3 Shearing Device

The last variable analysed is the one concerning the shearing device. So, for the same load, 200kPa, the same test was done with the GDS device and Standard Configuration machine. Of course, comparing results obtained from different devices can be misleading, because many variables should be considered. In *Figure 5.5* are reported the two resulting curves, obtained after the test, in terms of horizontal stress-horizontal displacement.

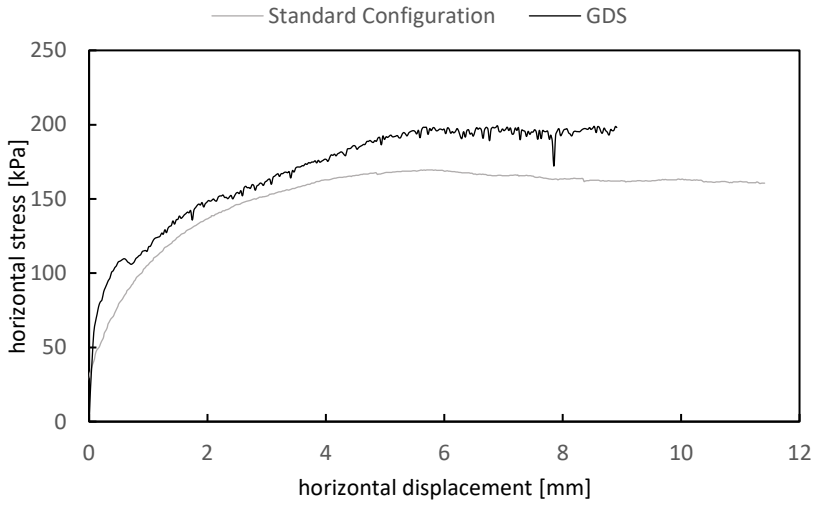

Figure 5.5 – Comparison between shearing response obtained with two different devices

Afterall, the obtained behaviour is very similar, the curves have the same shape, although the peak value difference is not negligible. A possible explanation could be related to the missing interface area correction, during shearing phase, in the Standard Configuration machine, therefore leading to lower shear stresses.

5.3 Preliminary Tests Under Suction Control

The objective was now to find a way to pursue the same shearing test procedure done with the hygroscopic samples, under suction control, thus without losing or gaining any suction/water content.

To this purpose it can be important to specify that bentonite clays are very susceptible to environment changes, hence not applying any control over suction along the test duration leads to huge water losses. What just stated was confirmed as a first preliminary test; a conditioned sample (total suction lower than hygroscopic suction) was tested with a vertical load of 1 MPa and a rate of 0.05 mm/min till a horizontal displacement of 9mm; over a duration of 3 hours and 20 min, the total suction value increased of 15 MPa.

The test confirmed what was imaginable, that is the necessity to create a sealed environment in order to isolate the shear box from the surroundings, recreating also inside this environment a target relative humidity, guarantying a steady suction value for the whole duration of the test, leading to results of shear strength and cohesion representative of that condition.

5.3.1 First Configuration

The “chamber” is realised thanks to a thermo-plastic bag, in the first steps of the test (≈20min) this will be sealed with scotch tape, due to the need to interact directly with the screws of the shear box; afterwards the sealing is realised with a vacuum sealer. Inside the available space in the shear box, two small jars containing the saturated saline solution (for the preliminary tests just NaCl) are positioned, those are the ones that will guarantee the relative humidity.

The configuration with the sealed plastic bag is reported in *Figure 5.6*.

Figure 5.6 – Front and side view of the sealed shear box

In the following a brief description of three different tests conducted with this configuration, in the attempt of assessing the feasibility of suction steadiness for the time needed to perform a shear test:

1. One test with sealed environment and jars containing NaCl saturated saline solution
2. One test with sealed environment and jars containing NaCl saturated saline solution, with an intermediate pause of 2 hours between consolidation and shearing
3. Regular shearing without sealed environment, for reference

After these three tests it was possible to conclude:

- The two hours pause between consolidation and shearing was effective to its purpose, which was allowing stabilization of relative humidity inside the sealed plastic bag and so within the soil sample
- This setup allows for maximum shearing displacement of 6mm, bringing to low levels of accuracy and confidence in the evaluation of peak and shear strength

5.3.2 Second Configuration

Since the interest was to find a good and reasonable coupling between the suction control and the reliability of the mechanical resistance parameters, another configuration was researched. The solution was found positioning the jars, containing the saturated saline solution, outside the shear box, assuring their steadiness with plastic regulable strips.

The setup is reported in *Figure 5.7*.

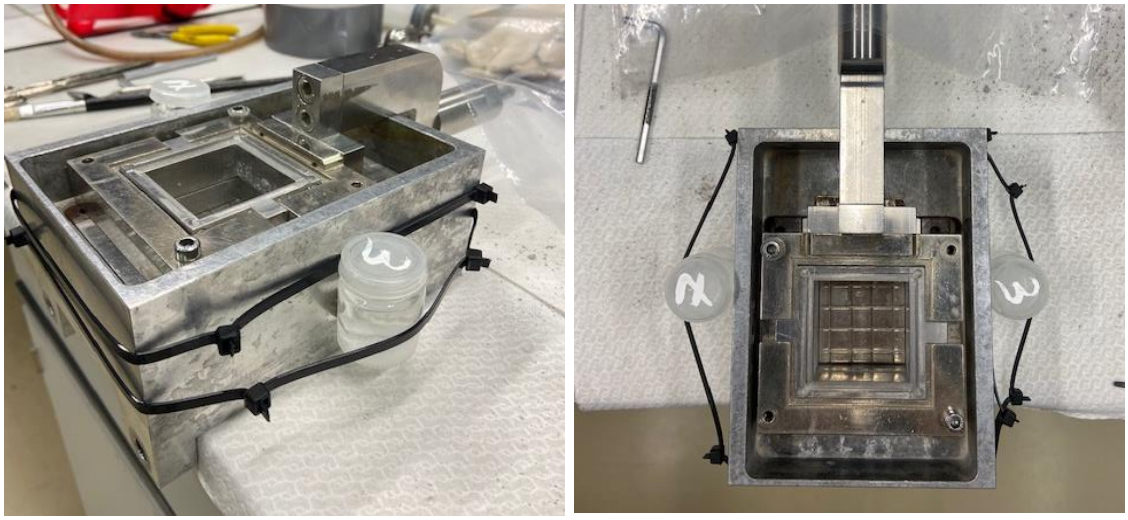

Figure 5.7 – Final shearing configuration

The trial testing with this configuration lead to the conclusion that the setup was reliable and effective.

5.4 Results

The results obtained, refer to the 45x45 shear box configuration, with a 0.05mm/min shearing rate and the GDS device.

In the following paragraphs the results are presented according to the following charts:

- Evolution of void ratio upon compression on $\log(\sigma_v)$-e plane

- Shearing response on the δh- τ plane
- Shearing response on the δh- δv plane
- Peak and ultimate failure envelopes

The reasons behind the first graph can be found in the attempt of evaluating the yield stress of the soil for every suction level investigated. In the final discussion the goal will be to foresee and highlight some possible trends of the mechanical characteristics of the tested material according to the suction variations.

5.4.1 Hygroscopic Results

The results are presented and furtherly discussed in the final paragraph.

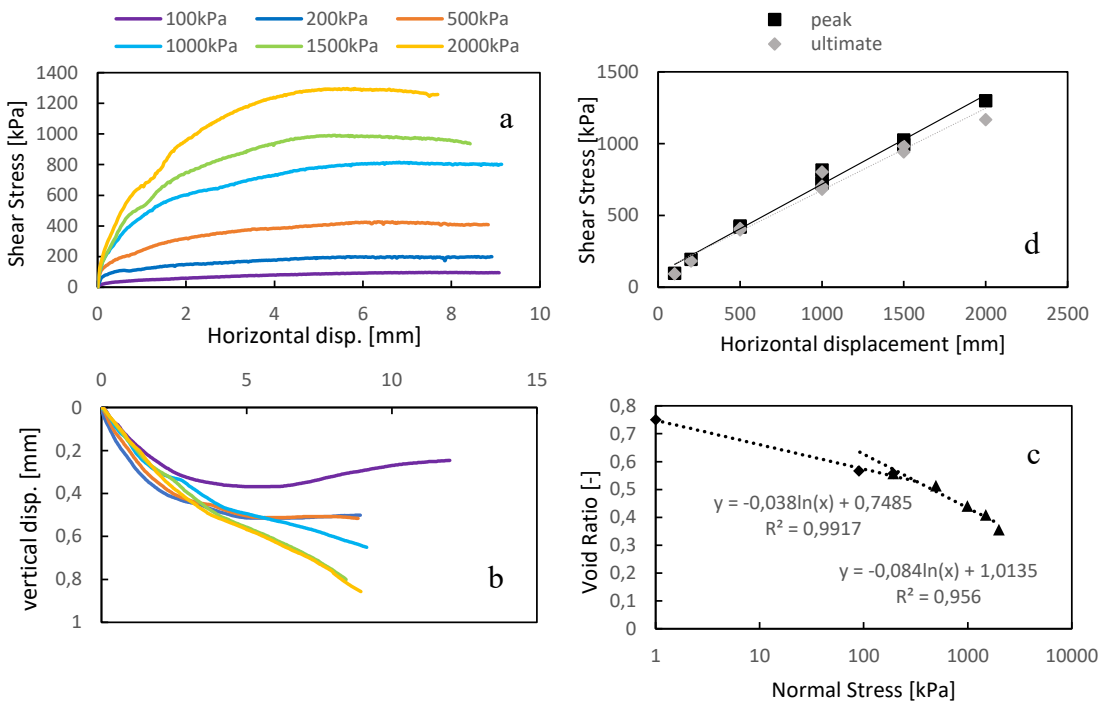

Figure 5.8 – a) Shear stress response in hygroscopic conditions for the six loads investigated; b) Response upon shearing in the displacement plane, for hygroscopic conditions, under the six loading conditions; c) Bilinear interpolation in the e-log(σ) plane to estimate yield stress; d) Peak and ultimate failure envelopes for bentonite in hygroscopic conditions

From Figure 5.8 c) it's possible to undersee a point of change in the steepness of the curve, being around 350 kPa, from a theoretical point of view this change shows that the soil crosses the elastic threshold and so that the virgin yielding behaviour begins.

We can search for consistency of what just said, looking at the evolution of both horizontal stress with horizontal displacement and horizontal displacement versus vertical displacement. In the same Figure 5.8 a) it is possible to see a slight change in behaviour in the sample, for the first three tests, so till 500kPa, the curves show no peak behaviour and after we can see a peak value and then an ultimate value. Verification of that can be found in Figure 5.8 b) in terms of horizontal displacement-vertical displacement, the soil reacts first with a contraction and then a dilation under loads lower than 500kPa, than changes behaviour over 500kPa, showing just a contractive behaviour.

Last graph reported in Figure 5.8, being d), was obtained through linearisation of the points reported in the τ-σ plane, to obtain friction angle and cohesion, according to Mohr Coulomb failure criteria:

$$\tau = c + \sigma_v * tan\varphi \tag{5.1}$$

Where the value of the apparent cohesion will be an intercept cohesion and the value of friction angle will be given by the slope of the linear envelope.

	φ[°]	c [kPa]
PEAK	31.8	96.8
ULT	30	106

Table 5.1 – friction angle and cohesion

Here, even if a linear envelope is used to represent the peak behaviour, it is possible to glimpse a non-linear behaviour, which is expected to actually better fit the results since the linearization of the failure envelope is a rather strong simplification.

5.4.2 Suction Control to 40 MPa

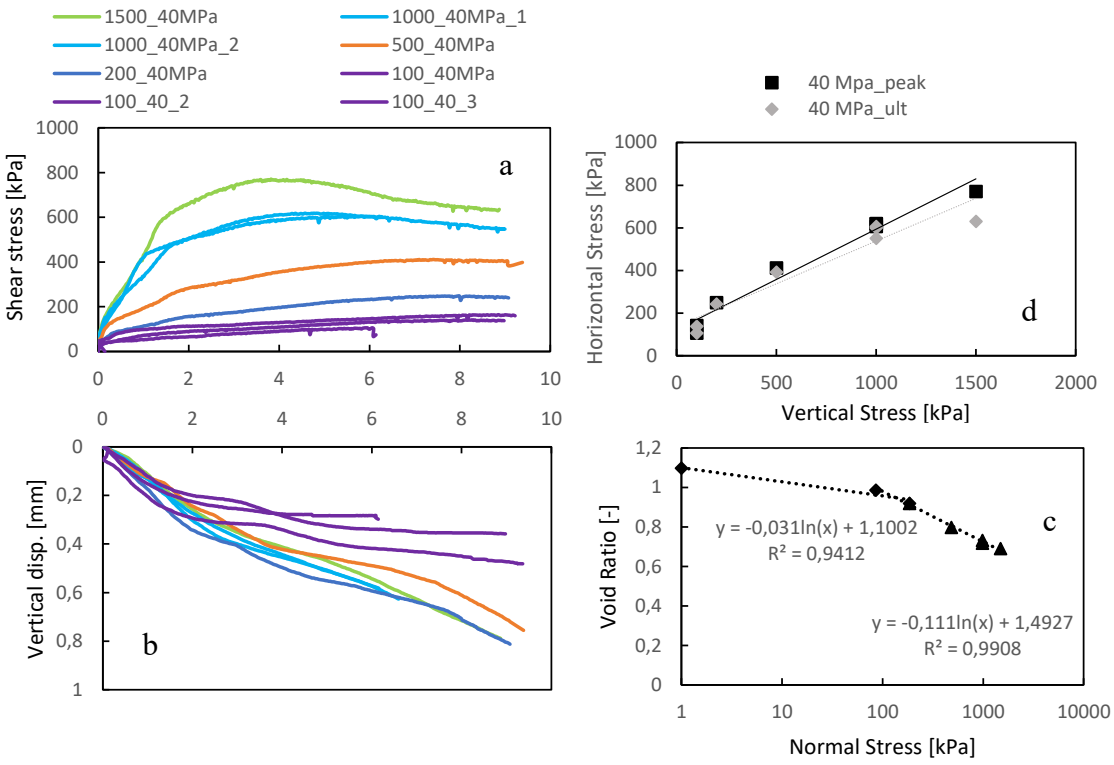

Figure 5.9 – a) Shear stress response for s= 40MPa and the five loads investigated; b) Response upon shearing in the displacement plane, for hygroscopic conditions, under the six loading conditions; c) Bilinear interpolation in the e-log(σ) plane to estimate yield stress; d) – Peak and ultimate failure envelopes for bentonite at s=40 MPa

	φ[°]	c [kPa]
PEAK	25.3	122
ULT	21.8	138

Table 5.2 – friction angle and cohesion at 40 MPa

5.4.3 Suction Control to 16 MPa

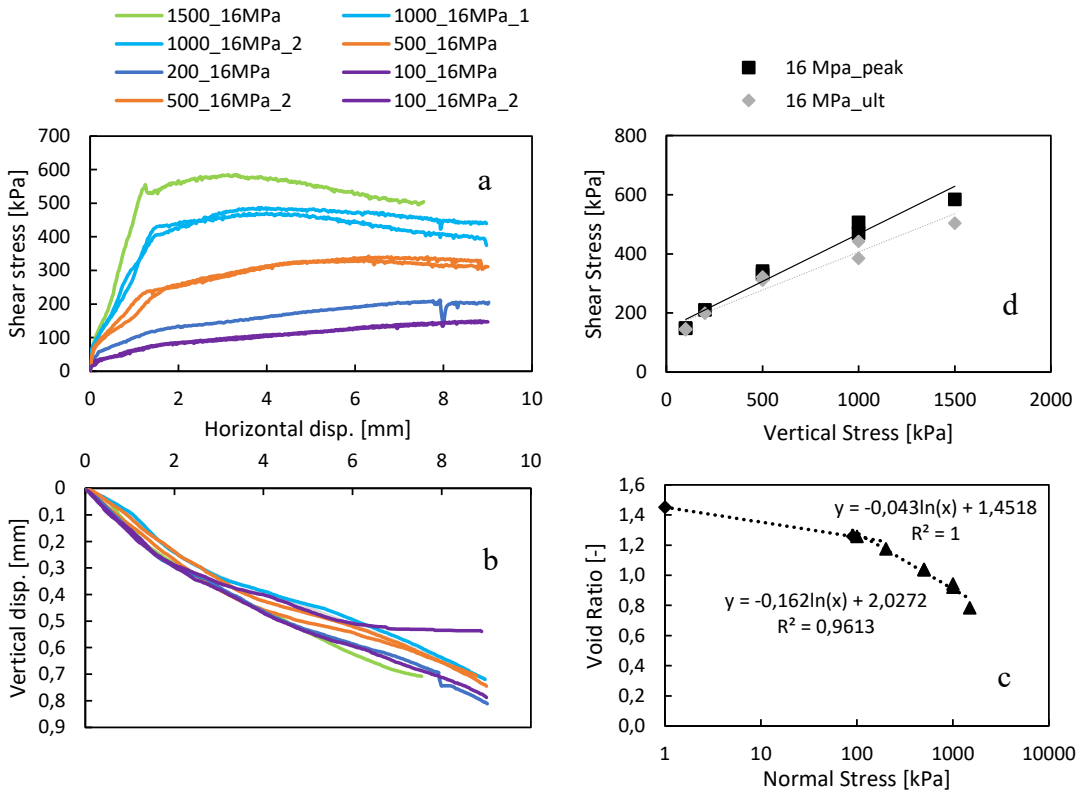

Figure 5.10 – a) Shear stress response for s= 16 MPa and the five loads investigated; b) Response upon shearing in the displacement plane at s= 16 MPa for the five loads investigated; c) Bilinear interpolation in the e-log(σ) plane to estimate yield stress; d) Peak and ultimate failure envelopes for bentonite at s=16 MPa

	φ[°]	c [kPa]
PEAK	17.8	146.1
ULT	14.5	148.9

Table 5.3 – friction angle and cohesion

5.4.4 Discussion

Now it is possible to put together the shearing response found under different suction levels, seeking for a general understanding and some consistence of the mechanical property's variations, eventually looking for explanations for the evidence found.

The first plot analysed concerns the yield stress, as reported in *Figure 5.12*. From this graph is possible to gain information about the trend followed by the soil sample subjected to variations in water content.

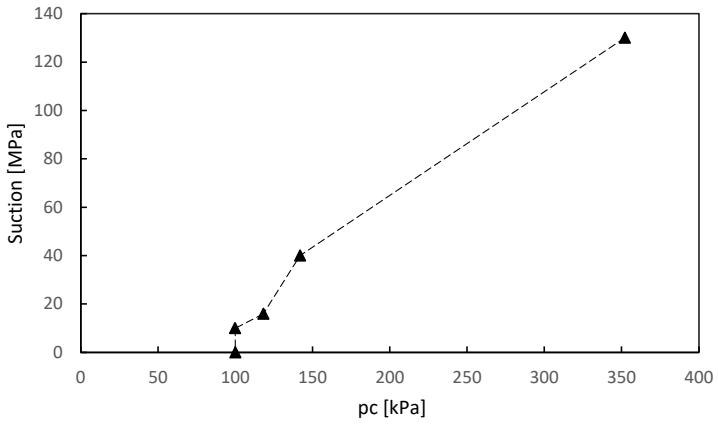

Figure 5.12 – Yield stress variation with suction

The bilinear interpolation performed for each suction level and reported in the paragraphs before allowed to individuate mathematically the point in which there is a change in slope of the curve and so a change in the behaviour of the soil subjected to vertical load.

Therefore, each graph allows to calculate the intercept between the two lines, which represent the yield stress for that suction level, we can then plot this values vs the suction at which they were found, to obtain the trend reported in *Figure 5.12*.

Similar results were found by Ye et al. (2012) through oedometric testing under both matric suction and temperature control, specifically they found an increasing trend of the yield surface with increasing matric suction value.

In the following *Figure 5.13* is represented the shearing response in terms of shear stress vs horizontal displacement, for the three datasets.

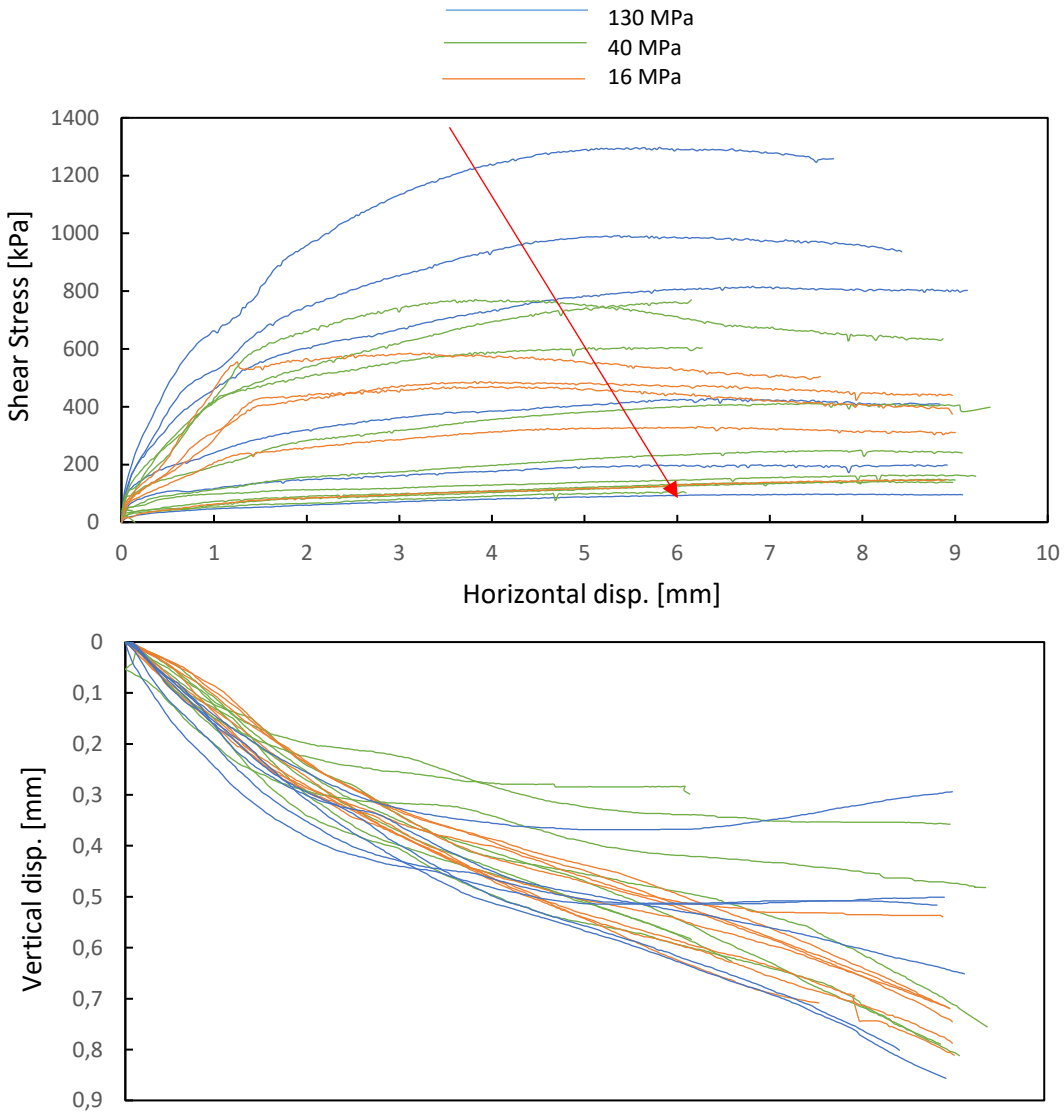

Figure 5.13 – Shearing response of all the suction and loads investigated

Overall, the response upon shearing in the δh- δv plane is contractive for all the suction levels and loads investigated.

From the same plot it is also possible to foresee a decreasing trend of the horizontal stress with increasing water content therefore decreasing total suction value.

To observe the same trend but decreasing the size of the focus, in the following *Figure 5.14* are reported the values of shear stress collected for one specific load, but different suction.

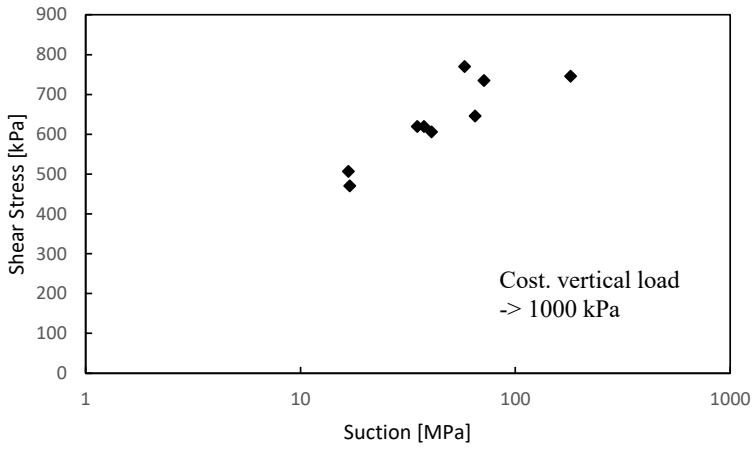

Figure 5.14 – Shear stress trend with suction

It can be clearly observed the dependency of shear stress detected with total suction value, where the best interpolating line is given by a power law. Last plot of interest is the one representing the failure envelopes, peak and ultimate, for the three datasets, as reported in *Figure 5.15*.

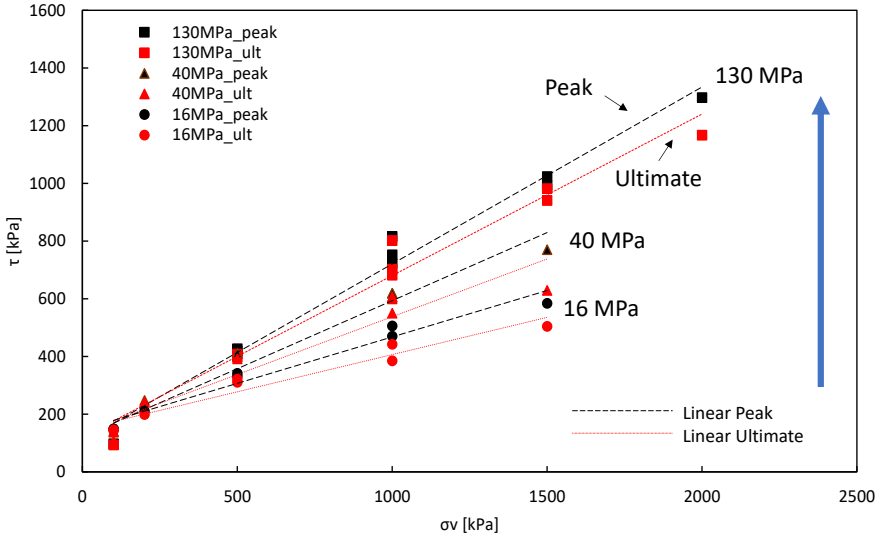

Figure 5.15 – Peak and ultimate failure envelopes for bentonite for all the suction levels investigated

Form this final representation it can be pointed out a trend in shear strength characteristics, the highest couple of envelopes is the one obtained in hygroscopic conditions, the middle couple is the one relative to a suction level of 40 MPa, whilst the lowest couple of envelopes is the one derived in the lowest suction level investigated, 15 MPa.

Hence, through linearisation of the envelopes it was possible to obtain mechanical parameters such as the friction angle and the cohesion for the three datasets, as reported in *Table 5.4*.

	PEAK	
	φ [°]	c [kPa]
130 Mpa	31.8	96.8
40 Mpa	25.3	122.0
16 Mpa	17.8	146.1
	ULTIMATE	
	φ[°]	c [kPa]
130 Mpa	30	106
40 Mpa	21.8	138.0
16 Mpa	14.5	148.9

Table 5.4 – Shear strength parameters for the three datasets

5.4.5 Effective Stress attempt

Thanks to the values collected for each test, it is possible through the following relation to evaluate the degree of saturation:

$$w * G_s = e * S_r \tag{5.2}$$

Where:

- Specific gravity $G_s = 2.74$
- e void ratio, depends on the loading conditions and on the suction level of the performed test

A differentiation was done concerning the *e* values, in particular the value right after load application was used to assess the peak failure envelope whilst the final *e* value (after shearing) was taken to evaluate the ultimate failure envelope, for each suction level.

Then the previously explained Bishop's formulation was used to evaluate effective stresses:

$$\sigma'_{v-ij} = \sigma_{net-ij} + sS_r\delta_{ij} \tag{5.3}$$

However, the above reported effective stress formulation was expected not to give the best fit for a bentonite, due to impossibility to account for the complex adsorption mechanisms that characterize this soil. Furthermore, those formulation refer to matric suction values and not total suction values.

For better comprehension, in *Figure 5.16* are reported the peak and ultimate failure envelopes obtained with Bishop's formulation.

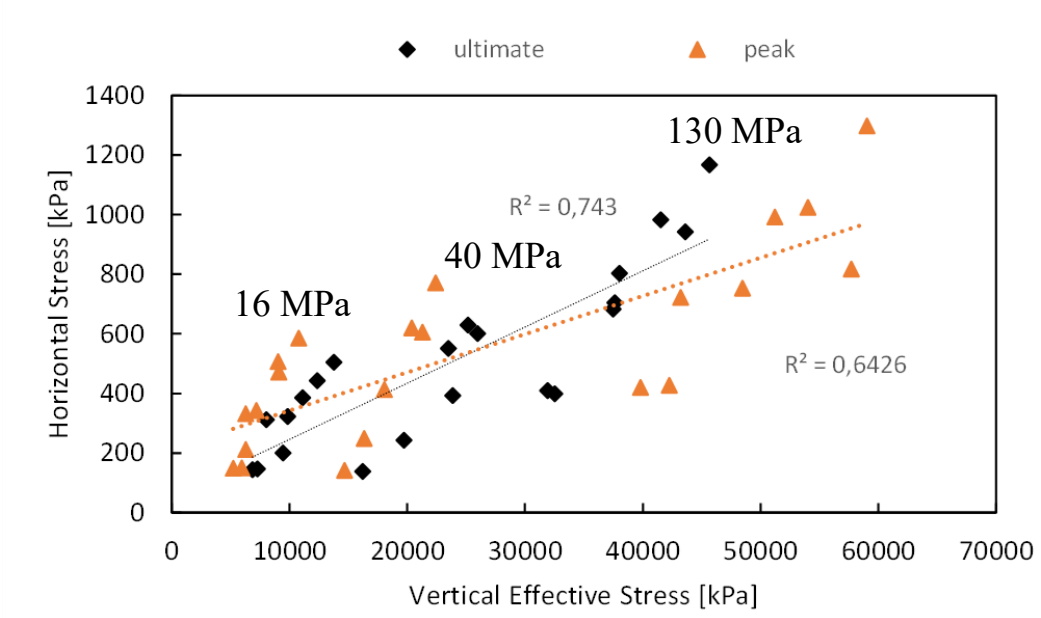

Figure 5.16 – Ultimate failure envelope in terms of effective stresses according to Bishop's formulation

One of the advantages of transforming total stresses into effective stresses, among those reported in theoretical framework in chapter 3, is the formation of a unique ultimate

failure envelope, leading to a unique couple of mechanical strength parameters, such as the effective friction angle and the effective cohesion. From *Figure 5.24* it can be seen that the values obtained according to this formulation do not return a clear trend.

One of the causes of this output is linked to the use of total suction, since values are very high if compared with total stresses applied, therefore bring to results governed by suction.

Another attempt was done to fit the total stress results in terms of effective stresses, using Tuttolomondo's formulation (2021), valid for sodium based bentonite. In the following reported equation (5.4) the introduced term, effective solute suction, is meant to account for the interactions between pore water and clay minerals, with the intent of scaling down the matric suction contribution to effective stresses.

$$\sigma'_{ij} = \sigma_{net-ij} + S_r(s_m - s_{s,e})\delta_{ij} \tag{5.4}$$

In the following the explanation of computational steps needed to apply effective stress formulation.

The $s_{s,se}$ terms was evaluated following two different strategies:

- Graphical evaluation
- Analytical evaluation

The graphical evaluation was pursued using the graph reported in Tuttolomondo et al. (2021) representing the solute suction of NaCl solutions with various NaCl concentrations, reported in the following *Figure 5.17*.

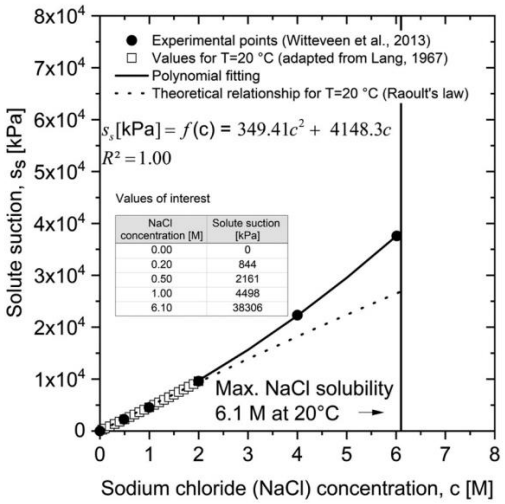

Figure 5.17 - Evolution of Solute suction with sodium chloride concentration increase (Source: Tuttolomondo et al., 2021)

A sample of bentonite was saturated and, under the assumptions of Sr=1, the value of $s_{s,pw}$ of the sample was evaluated through WP4C device.

It was necessary to acknowledge the matric suction, starting from total suction value. A common assumption in the unsaturated field is to consider the total suction as given by:

$$\psi = s_m + s_o \tag{5.5}$$

Where s_m is the matric suction and s_o is the osmotic suction; it is important to highlight that this definition is an assumption, yet not fully validated but widely used. With the tools available, the strategy to evaluate s_o was to saturate a bentonite sample and measure the water potential through WP4C device; in such conditions (S_r=1) it can be stated that total suction = osmotic suction. In *Figure 5.18* is reported a picture of the saturated sample positioned inside the microcell, from which is water potential will be evaluated.

Figure 5.18 – Saturated bentonite sample

Thus, from this sample the water potential value was measured equal to -0.33÷0.38 MPa, together with the correspondent water content being of ≈ 80%.

Entering the graph reported in *Figure 5.17* with this value, it was possible to obtain the relative NaCl concentration. Known the volume of water of the relative bentonite sample:

$$c = \frac{n_{mol}}{V_w} \tag{5.6}$$

It was possible to obtain the number of moles of NaCl contained in the pore water. This number can be considered constant for all the samples analysed, since during vapor equilibrium technique treatment what is changing within the specimen is only the water amount, thanks to the vapor exchange.

Hence, using the inverse process, starting from water content values it was possible to obtain the concentration of NaCl relative to each test performed, leading to the final estimation of $s_{s,pw}$.

Once know this value, $s_{s,e}$ was easily estimated as difference between $s_{s,pw}$ and s_o, under the assumptions of pure demineralized water this value was considered equal to zero therefore $s_{s,pw} = s_{s,e}$.

Lastly the matric suction was evaluated as a difference between total suction value and the solute suction of the pore water in the system.

Unfortunately, no changes in the effective envelopes obtained from the usage of this method are obtained, as can be seen by the failure envelope reported in *Figure 5.19*.

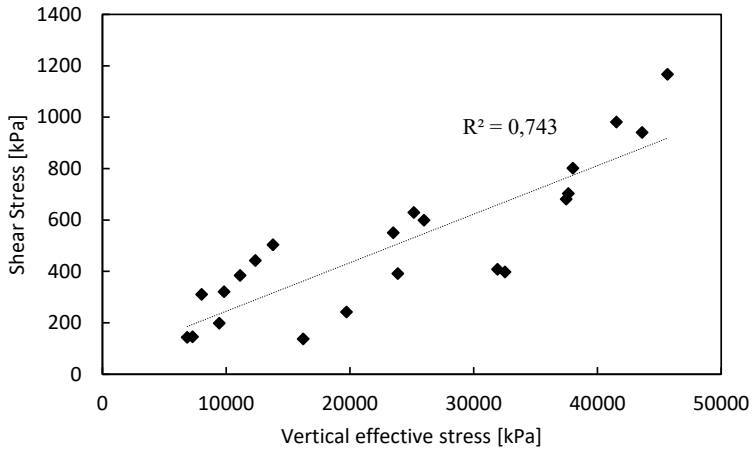

Figure 5.19 – Ultimate Failure envelope obtained by mean of Tuttolomondo's formulation

Secondly the estimation of $s_{s,se}$, was done through a pre-setted Matlab code.

The input information needed to use the code are listed below:

- CEC, cation exchange capacity
- Void ratio
- Degree of saturation
- Soil particle density

The cation exchange capacity is a function of mineralogical composition of the clay, specifically it is given by the product of the mineral fraction times the CEC value of the pure mineral. The mineral fraction, in particular the smectite content was taken from Seiphoori (2014) and the CEC relative of smectite was taken from literature (Mitchell and Soga, 2005).

Then each value of $s_{s,pw}$ is evaluated using experimental data and for an imposed δ value. This parameter can be approximated as a material parameter, a first evaluation can be done thanks to the empirical formulation:

$$\delta = 0.0009CEC + 0.0815 \tag{5.7}$$

Which for the studied case leads to a value of 0.146. Nevertheless, four different values of δ were taken: 0.5, 0.15, 0.2 and 0.3, with the intention of optimizing the fitting and the effective stress values. The results obtained for each δ are reported below in *Figure 5.20*.

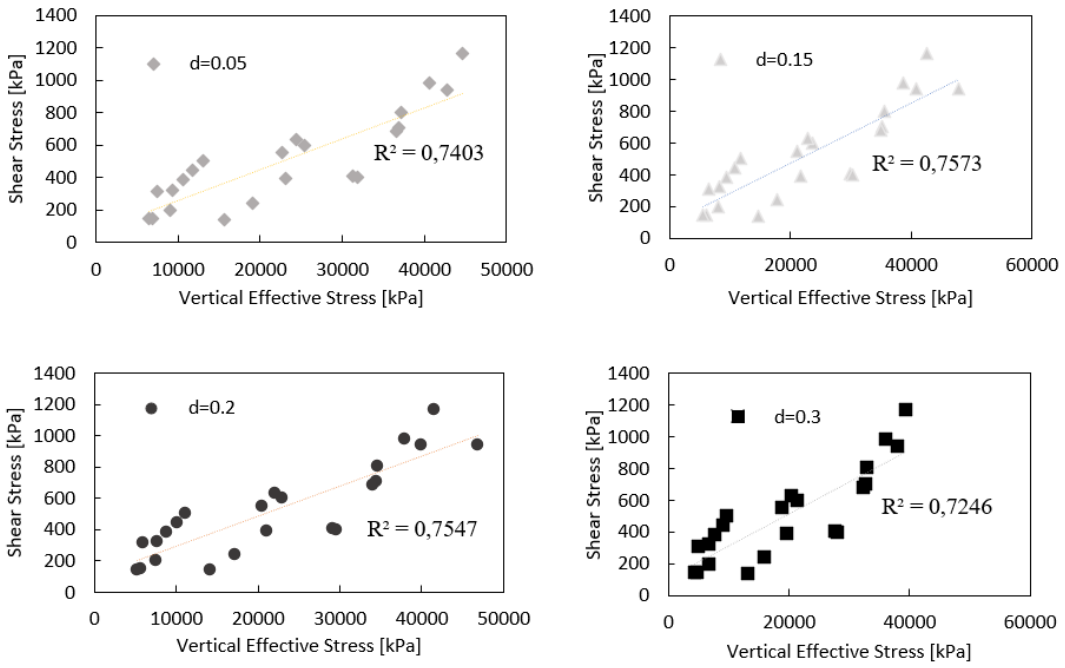

Figure 5.20 – Ultimate Failure envelope obtained by mean of Tuttolomondo's formulation with 4 different values of δ

Very slight improvements in the fitting can be achieved if moving from Bishop's formulation to a formulation that considers bentonite's activity, thus Tuttolomondo's formulation, with particular reference to the data obtained through the second method i.e.

Nevertheless, this output should not be linked to the non-effectiveness of Tuttolomondo's formulation to describe the behaviour, instead to the unreliability of matric suction values obtained by back calculation from total suction values.

To date, this appears to be a hot topic, as the problem of switching from total suction to matric suction has been widely encountered. In fact, what many researchers are highlighting is the possibility of a missing term in the previously reported equation (5.5), leading therefore to higher values of matric suction if back calculated from it. As a

consequence, those matric suction values both are not reliable and not representative of the actual state of the soil.

In general, it can be stated the difficulty of reasoning in terms of effective stresses when experimental data come from unsaturated direct shear testing, due to lack of control over the interstitial pressures developing withing the sample, while shearing.

It is indeed possible to achieve in the effective stress evaluation in unsaturated direct shear testing, when the shear box setup is modified in such a way to control and impose matric suction over the sample (Hamid and Miller, 2009).

A suggested strategy could go through the usage of MIP (Mercury Intrusion Porosimetry), as a mean of evaluating matric suction. More into details, this technique allows for the evaluation of pore size distribution (PSD) of a soil, a sample is injected with a non-wetting fluid, mercury, and both the pressure and volume of mercury are measured along the test. Then, the results in terms of mercury's surface tension can be transformed thanks to Young-Laplace equation – reported below – into water's surface tension, ergo into matric suction, and the volume injected can give reference of the degree of saturation. The derived water retention curve is in the domain of a main drying curve.

$$s = -\frac{\gamma_w cos\vartheta_w}{\gamma_{Hg} cos\vartheta_{Hg}} p_{Hg} \tag{5.8}$$

Where γ_w and γ_{Hg} are the surface tension of water and mercury, and the ϑ values refer to contact angles of mercury-air system and water-air system.

The derived matric suction values could be used to compare with results obtained from back calculation, and then lastly to calculate effective stresses.

6. Strength Characteristics of Steel-Bentonite Interface

The goal of this thesis was the realisation of these final set of tests, where the coupling between all the afore mentioned processes can be seen in one unique testing setup.

Indeed, the previous chapter for shear strength evaluation under different suction conditions was necessary as a reference, to put the bases of the shearing response of the soil, to be able to compare the mechanical parameters got with the behaviour of the soil in interface testing.

In this last experimental investigation, the purpose was to move the focus from pure soil behaviour to the coupling obtained if introducing another variable, the steel interface.

6.1 Configuration of setup

A schematic diagram of the testing setup is reported in *Figure 6.1*; the configuration of the standard shear box was modified substituting the bottom perforated metal plate that allowed the fitting of the soil sample, with a steel plate with dimensions 105mmx60mm and a 16mm height, as reported in *Figure 6.2*. The design roughness of the steel surface is 16 μm, the approximate value of relative roughness is 0.002, leading to the assumption of smooth counterface.

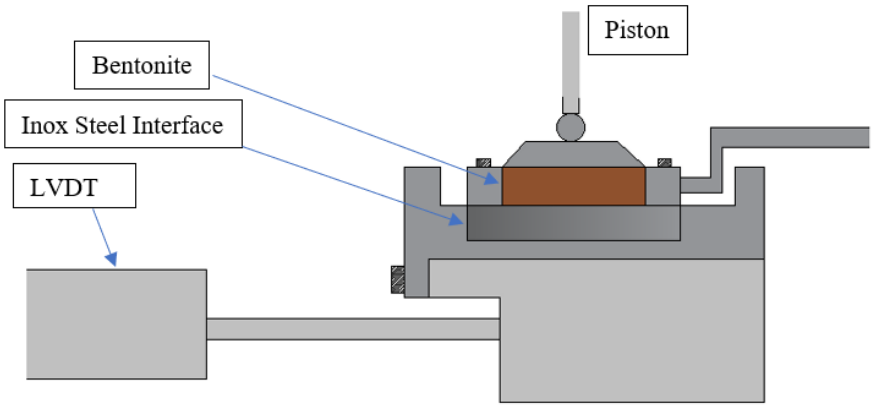

Figure 6.1 – Illustration of the shear box for interface testing

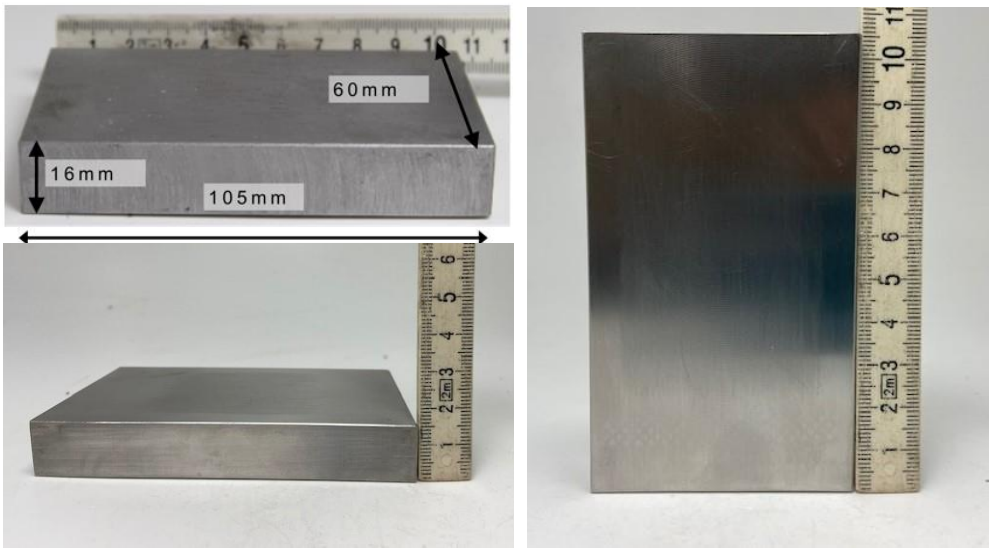

Figure 6.2 – Geometry of steel plate

Unlike the direct shear test, the contact area can be considered constant during the friction testing, so it is not necessary to correct the contact area during shearing.

The test to be performed are two sets of five loads each, the first set will be performed in hygroscopic conditions, whilst the second set will be performed for a value of total suction of 15 MPa.

The first set was performed with a steel piece already present in the laboratory equipment, although when the first test under suction control was performed, corrosion was detected in the steel surface. Thus, another steel piece was ordered, with stainless characteristics.

6.1.1 Non-Stainless-Steel Interface

As above mentioned, during the first shearing test performed under suction control, as shown in the following pictures, corrosion took place.

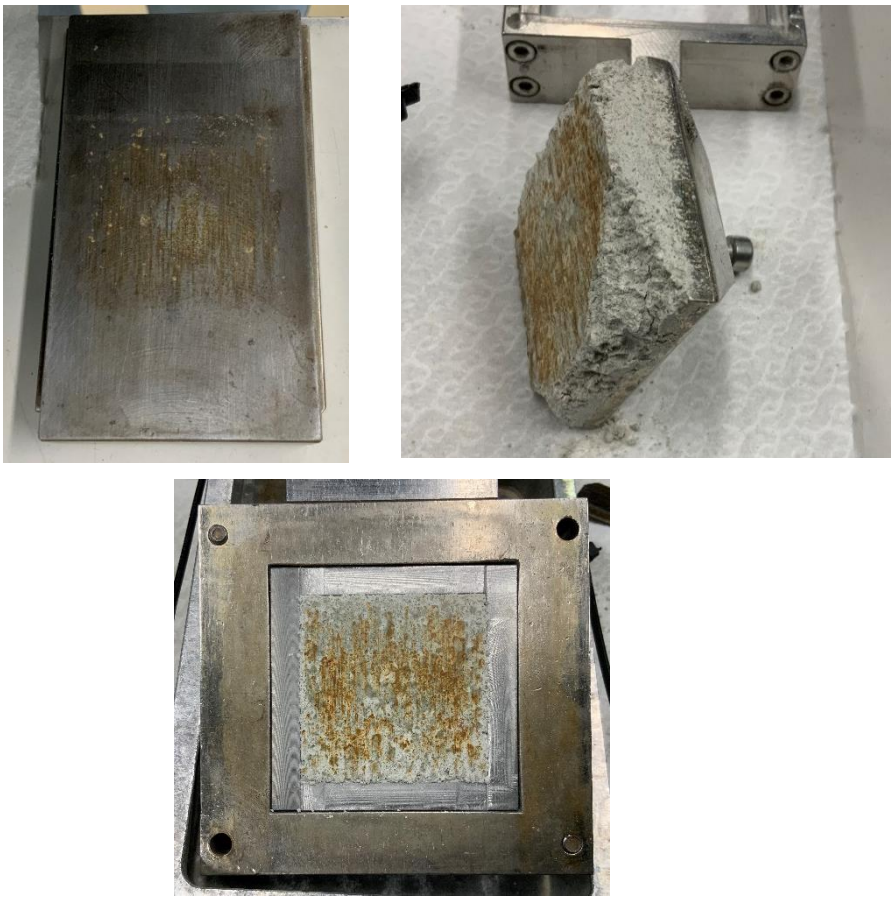

Figure 6.3 – Corrosion observed on the steel surface and soil sample

From *Figure 6.3* is possible to see a homogenously distributed orange halo over the soil surface; furthermore, on the steel surface not only the same halo was found, but also part of the sample – small lumps – were found attached to the surface.

Triggering causes:

- Water content of the specimen
- Salinity of bentonite
- Oxidizable steel piece

Consequences:

- During the chemical reaction of corrosion bonds between steel and bentonite were created;
- It is possible to address the peak behaviour seen in the τ-δh plane (*Figure 6.4*) to this reason

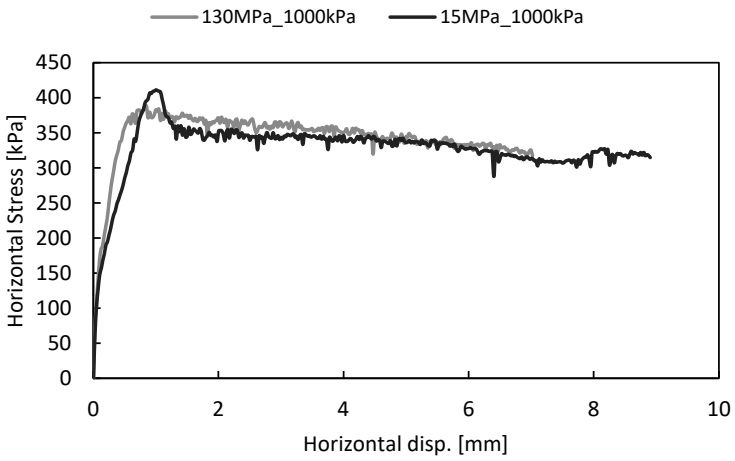

Figure 6.4 – Shearing response of corroded sample compared with hygroscopic interface shearing response

Also, as mentioned before some soil particles were found attached to the steel surface at the end of the test, hence it is possible that a fictitious roughness was introduced, leading to results difficult to safely compare with the hygroscopic behaviour.

6.2 Results

In the following paragraphs results of the two datasets are present separately and then discussed.

6.2.1 Hygroscopic Results

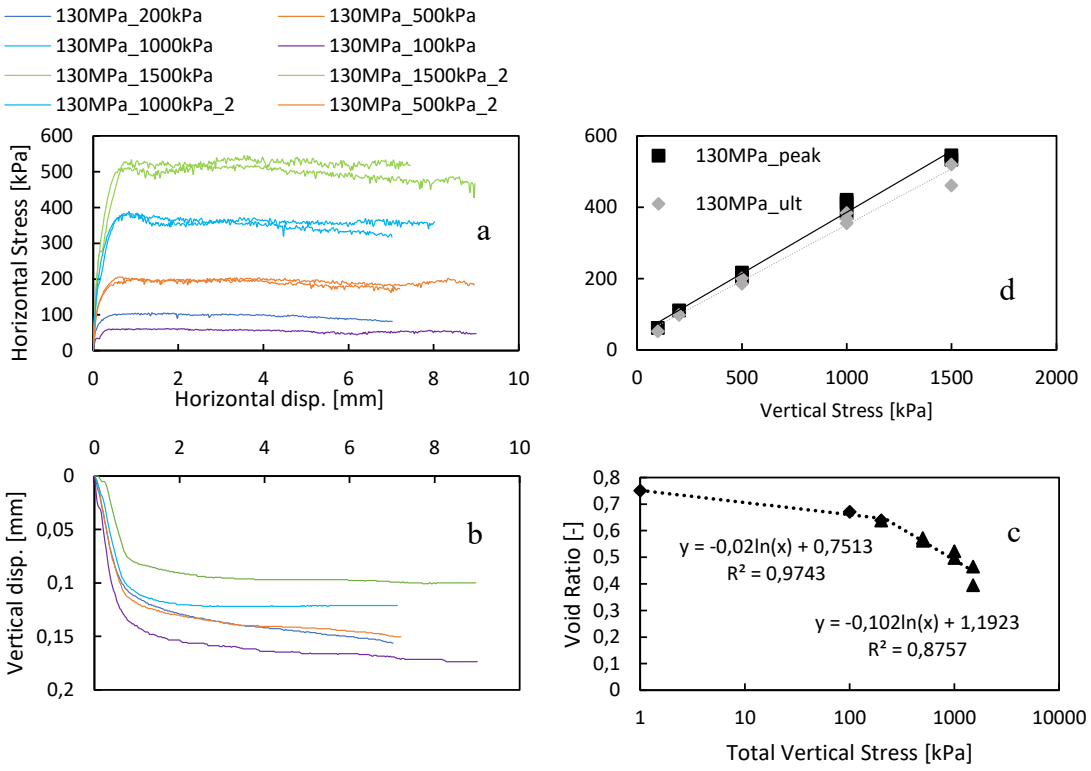

Figure 6.5 – a) Interface shear stress response in hygroscopic conditions and for the five loads investigated; b) Response upon shearing in the displacement plane in hygroscopic conditions for the five loads investigated; c) Bilinear interpolation in the e-log(σ) plane to estimate yield stress; d) Peak and ultimate interface failure envelopes for bentonite for hygroscopic conditions

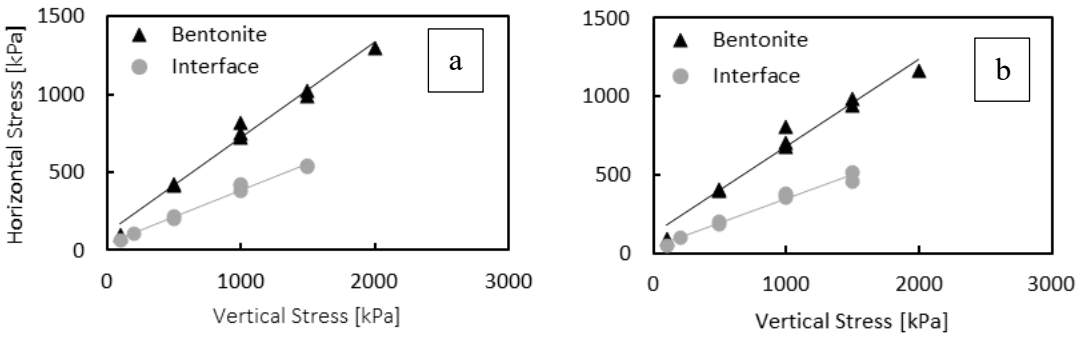

Figure 6.6 – a) Comparison between peak failure envelope for hygroscopic conditions among soil and interface; b) Comparison between ultimate failure envelope for hygroscopic conditions among soil and interface

From *Figure 6.6* in hygroscopic conditions, a great decrease in friction angle is recorded from internal to interface, both for peak and ultimate failure envelopes. As it is known that interface friction angle is lower than internal friction angle for soils (Lancellotta, 2008), therefore results could have been predicted.

In the above reported results, it is possible to notice that three tests were repeated with the new steel interface, respectively of the three following vertical loads: 500 kPa, 1000 kPa and 1500 kPa. According to the results found in terms of horizontal stress vs horizontal displacement and in terms of failure envelops, it is safe to conclude that no great difference is detected, values for the second steel plate are slightly higher, this information can be interpreted to drive conclusions about the roughness of the new piece, specifically, as reported previously in chapter 1, higher shear resistance is typically associated with higher roughness of the counterface.

6.2.2 Suction Control to 15 MPa

Since the steel plate used for the first set of tests was found corroded after performing the first shearing test at 15 MPa suction level, another was realised in stainless steel. The following results are obtained according to this new interface.

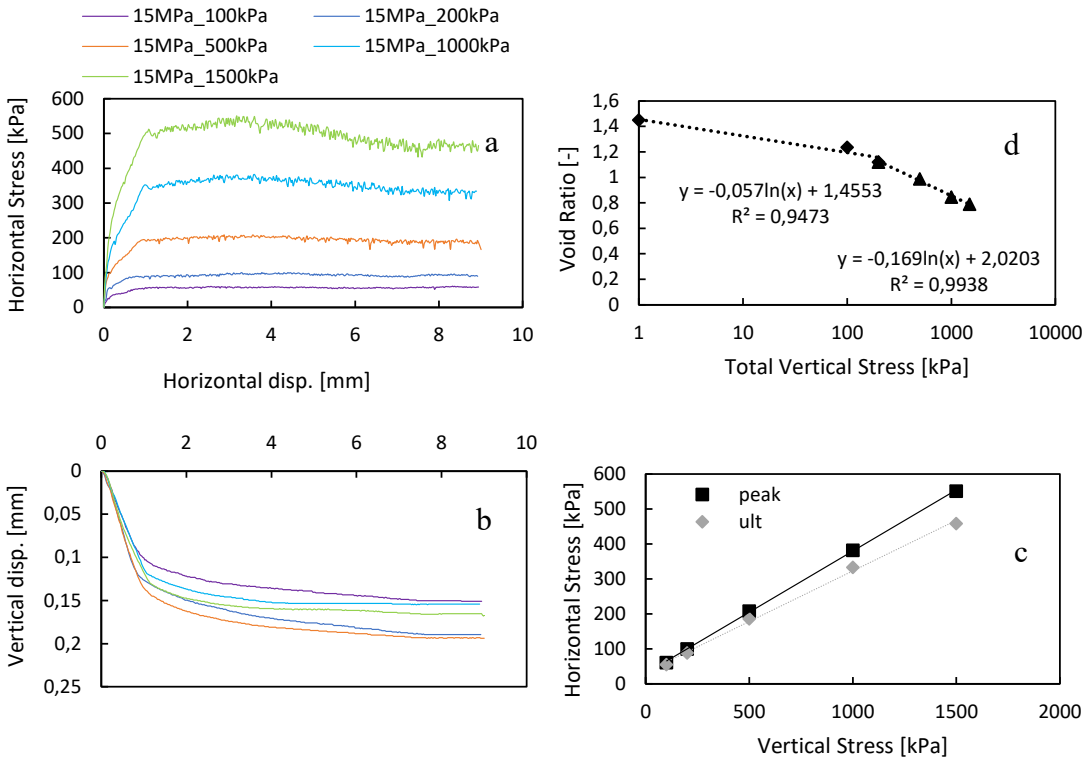

Figure 6.7 – a) Interface shear stress response at s= 15 MPa for the five loads investigated; b) Response upon shearing in the displacement plane at s= 15 MPa for the five loads investigated; c) Bilinear interpolation in the e-log(σ) plane to estimate yield stress; d) Peak and ultimate interface failure envelopes for bentonite for s= 15 MPa hygroscopic conditions

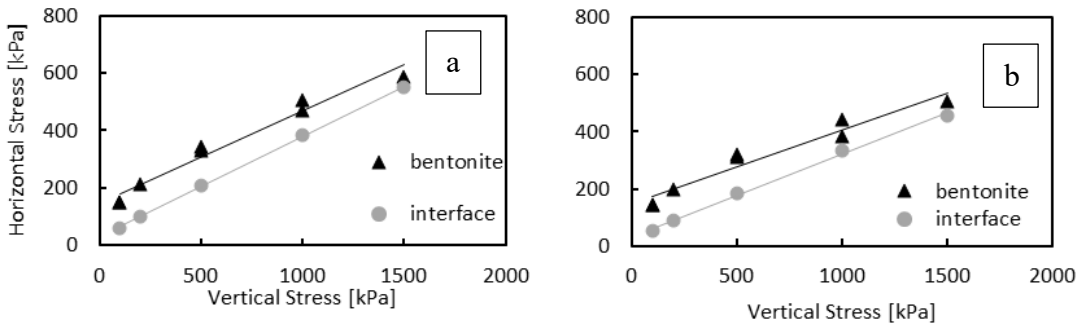

Figure 6.8 – a) Comparison between peak failure envelope for s= 15 MPa among soil and interface; b) Comparison between ultimate failure envelope for s= 15 MPa among soil and interface

The interface friction angle obtained under 15 MPa suction level, if compared with internal friction angle as shown in *Figure 6.8*, result to be quite similar leading to the initial assumption of a soil-soil failure. As reported previously in Chapter 1.3, this behaviour was studied by Tsubakihara and Kidasha in 1993, through direct shear testing they stated the existence of a critical roughness value, above which failure happens within the sample. Although the impossibility of assessing in the studied case the critical roughness value, it can be said that the evaluated relative roughness of the used steel surface is rather low, leading to the conclusion that failure did happen along the interface.

As a validation to the assumption reported above, samples were found to be highly compacted at the end of the test, showing the formation of a smooth and somehow cemented surface where the shearing had occurred. In the following *Figure 6.9* is reported a picture of a sample.

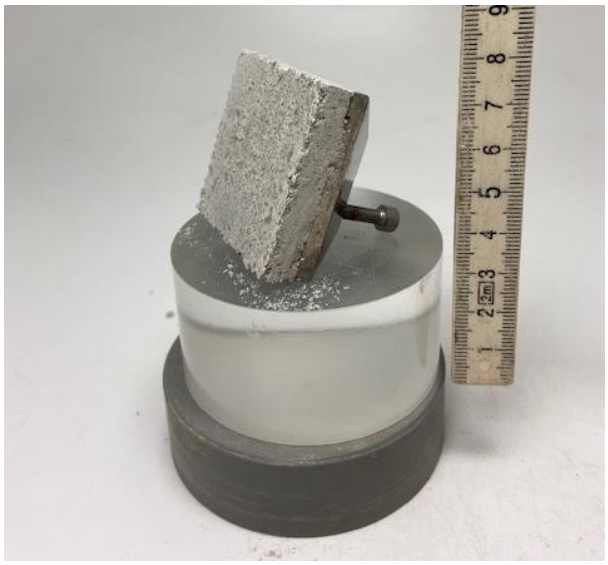

Figure 6.9 – Bentonite sample after interface shearing under s=15 MPa

6.2.3 Discussion

For the purposes of assuring comparability between the two set of tests, since they were performed with two different counterfaces, three shearing tests of the first set, with three different loads, were repeated and compared with previous results, as reported in *Figure 6.16*.

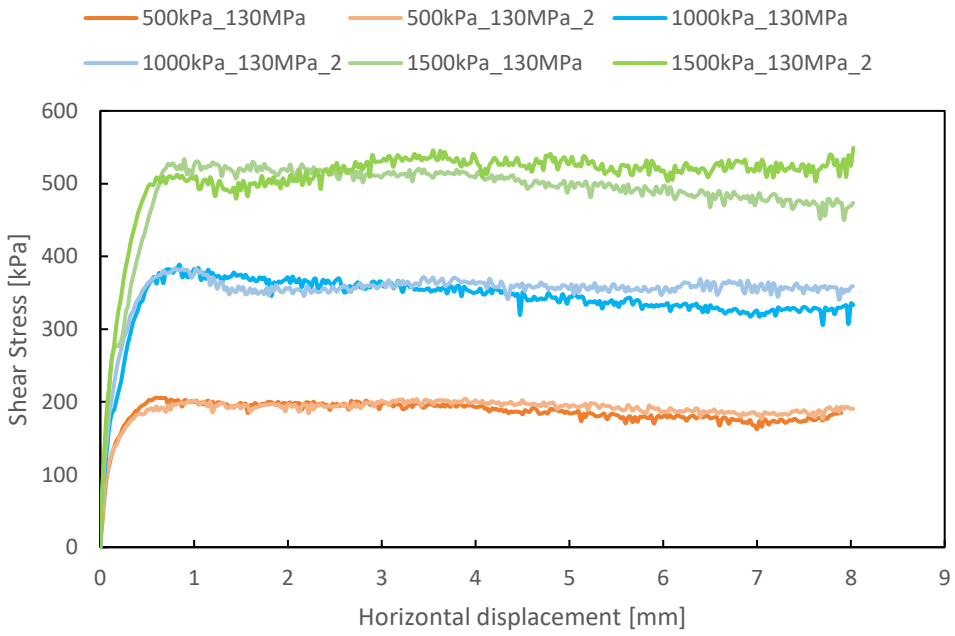

Figure 6.16 – Comparison between shearing between first and second steel counterface

From the plot reported above it can be seen that the shearing response in terms of shear stress appears to be slightly higher with the new steel plate, leading to the conclusion of a higher roughness. Overall, since the difference is not affecting the envelopes, it was decided to use all the values as if they belonged to the same set.

In the following *Figure 6.17* are reported: in the left plot all the failure envelopes – peak and ultimate – for interface testing; in the right plot a comparison between soil shearing response and interface response in terms of peak and ultimate failure envelopes. In *Table 6.3* are also reported values of the interface friction angle and the cohesion obtained for the two suction levels, compared with previous soil shear strength parameters.

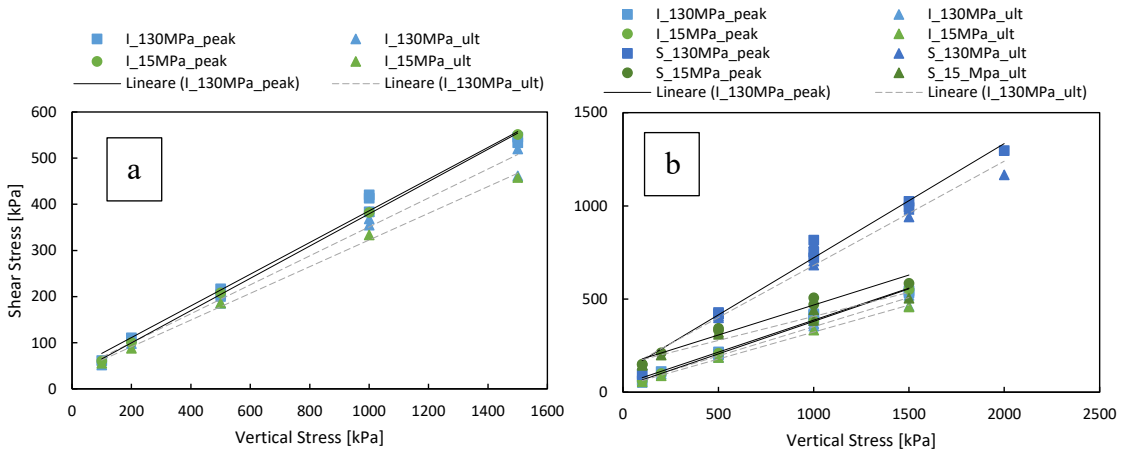

Figure 6.17 – Interface Peak and Ultimate Failure Envelopes for the two suction levels studied

SOIL					
130MPa			**15 Mpa**		
	ϕ [°]	*c [kPa]*		*ϕ [°]*	*c [kPa]*
peak	31.8	96.8	**peak**	17.8	146.1
ultimate	30.0	120,67	**ultimate**	14.5	148.9
INTERFACE					
130Mpa			**15 Mpa**		
	ϕ [°]	*c [kPa]*		*ϕ [°]*	*c [kPa]*
peak	18.9	42.5	**peak**	19.3	30.0
ultimate	17.4	37.2	**ultimate**	16.1	33.3

Table 6.3 – Cohesion and friction angle both for direct shear testing and interface testing, for the two suction levels investigated

The purpose of *Figure 6.17 a)* is to show that all the obtained envelopes are close to each other, with an upper limit formed by the hygroscopic peak envelope and a lower limit formed by the ultimate envelope at 15 Mpa total suction.

The proposed explanation of the similarities found between all interface results in terms of envelopes, under different total suction levels, is to be linked with a distortion of air-water menisci along the steel interface while shearing, leading to a reduction of effective contribution of suction to interface shear strength.

As reported before in Chapter 1.3, a similar trend was found by Hamid and Miller (2009) for Milco silt, they investigated interface behaviour through direct shear testing under

matric suction control, both for smooth and rough steel surface. The output of the campaign was that interface friction angle was not dependent of matric suction changes.

Concerning the yield stress evolution, it can be stated that the same trend as the one found for soil testing is confirmed; even in interface testing the preconsolidation pressure increases starting from initial air entry value, assumed equal to 10 MPa according to literature, to higher values following suction increase. This trend, reported in *Figure 6.19*, implies that with suction increase the soil sample will reach the plastic domain for higher vertical loads.

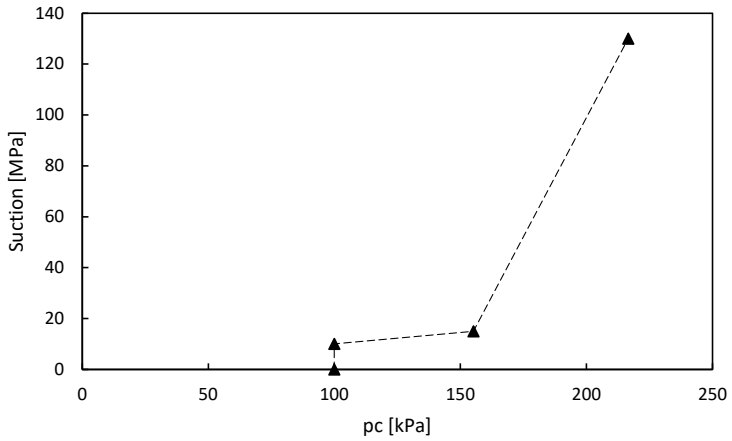

Figure 6.19 – Evolution of yield stress

The comprehension of yield stress evolution allows the prediction of the plastic domain, regardless of the impossibility to assess such behaviour in terms of effective stress, remains still valuable information.

7. Conclusion

This research work has been driven by the need to assess the variations of mechanical properties of importance for bentonite soil, if accounting for the boundary conditions of Nuclear Waste Disposal in the Swiss concept. Nowadays, a lot of research work has been done with both macro and micro-scale laboratory testing and numerical analysis to characterise the hydro-thermo-mechanical behaviour of buffer materials to improve understanding and design of deep geological repositories. This master thesis has been dedicated to the evaluation of the mechanical characteristics of steel-bentonite interface in hygroscopic conditions and under suction control conditions. The main challenge encountered was, from an experimental point of view, the ability to develop a testing procedure where total suction steadiness could be granted.

Through both internal and interface testing, using a modified configuration of direct shear test for different levels of total suction, the following conclusions were derived:

- Shear strength of bentonite was found to be suction dependent
- A clear trend of internal friction angle decrease was found, with decreasing total suction
- Intercept cohesion values appear to increase with decreasing total suction value
- Comparison between internal friction angle and interface friction angle showed that shear strength resistance is lower in interface testing, for hygroscopic conditions
- In this configuration, a decrease in total suction does not lead to a decrease in shear strength, therefore total suction is not controlling the interface shear resistance
- A unique envelope can be used to design the system

Some prospective of the thesis developed could be concerning the possibility of assessing the consistency of the findings, repeating the experimental campaign this time starting from fully saturated state and moving along the main drying, allowing also for comparison in terms of matric suction using Mercury Intrusion Porosimetry. This could give the chance of assessing either repeatability, consistency and lastly the possibility to interpret, in a reliable way, results in terms of effective stresses.

References

Alonso, E. E., Romero, E., Hoffman, C., & Gracia-Escudero, E. (2005). Expansive bentonite–sand mixtures in cyclic controlled-suction drying and wetting. *engineering geology*, 213-226.

Baldi, G., & Hueckel, T. (1990). THERMOPLASTICITY OF SATURATED CLAYS: EXPERIMENTAL CONSTITUTIVE STUDY. *Journal of Geotechnical engineering*, 1778-1796.

Blatz, J., Graham, J., & Chandler, N. (2002). Influence of suction on the strength and stiffness of compacted sand-bentonite. *Canadian Geotechnical Journal*, 1005-1015.

Blumling, P., Bernier, F., Lebon, P., & Martin, C. (2007). The excavation damaged zone in clay formations time-dependent behaviour and influence on performance assessment. *Physics and Chemistry of the earth2007*, 588-599.

bradbury, M., & Baeyens, B. (2003). Porewater chemistry in compacted re-saturated MX-80 bentonite. *Journal of contaminant hydrology*, 329-338.

Chen, W., Tan, X., Yu, H., Wu, G., & Jia, S. (2009). A fully coupled thermo-hydro-mechanical model for unsaturated porous media. *journal of rock mechanics and geotechnical engineering*, 31-40.

Chen, Y.-G., Dong, X.-X., Zhang, X.-D., Ye, W.-M., & Cui, Y.-J. (2021). Oedometric compression and thermal volume behavior of compacted Gaomiaozi bentonite saturated with salt solution. *Geomechanics for energy and the environment*.

Cordoso, R., Romero, E., Lima, A., & Ferrari, A. (2007). A Comparative Study of Soil Suction Measurement Using Two Different High-Range Psychrometers. *Experimental unsaturated soil mechanics*, 79-93.

Cullin, M., Birmingham, G., Swinivasan, R., & Hailu, G. (2020). Injectable Sodium Bentonite Inhibitors for Corrosion under Insulation. *ASCE*.

Dananaj, I., Frankovska, J., & Janotka, I. (2004). The influence of smectite content on microstructure and geotechnical properties of calcium and sodium bentonites. *Applied clay science*, 223-232.

Del Olmo, C., Fioravante, V., Gera, F., Hueckel, T., Mayor, J., & Pellegrini, R. (1996). Thermomechanical properties of deep argillaceous formations. *Engineering geology*, 87-101.

Di Donna, A., Ferrari, A., & Laloui, L. (2015). Experimental investigations of the soil–concrete interface: physical mechanisms, cyclic mobilization, and behaviour at different temperatures. *NCR Research Press*, 659-672.

Eigloffstein, T. (2001). Natural bentonitesFinfluence of the ion exchange and partial desiccation on permeability and self-healing capacity of bentonites used in GCLs. *geotextiles and Geomembranes* , 427-444.

Gleason, M., Daniel, D., & Eykholt, G. (1997). calcium and sodium bentonite for hydraulic containmen applications. *Journal of geotechnical and geoenvironmental engineering*, 438-445.

Hamid, T., & Miller, G. (2009). Shear strength of unsaturated soil interfaces. *NCR Research press*, 595-606.

Hu, L., & Pu, J. (2004). Testing and Modeling of Soil-Structure Interface. *journal of geotechnical and geoenvironmental engineering*, 851-860.

Hueckel. (1998). A constitutive study of thermo-elasto-plasticity of deep carbonatic clays. *International journal for numerical and analytical methods in geomechanics*, 549-574.

Hueckel, T., & Pellegrini, R. (1992). Effective stress and water pressure in saturated clays during heating-cooling cycles. *Canadian geotechnical journal*, 1095-1102.

Hueckel, T., Pellegrini, R., & Del Olmo, C. (1998). A constitutive study of thermo-elasto-plasticity of deep carbonatic clays. *Int. J. Numer. Anal. Meth. Geomech.*, 549-574.

Hueckel, T., Pellegrini, R., & Del Olmo, C. (1998). A CONSTITUTIVE STUDY OF THERMO-ELASTO-PLASTICITY OF DEEP CARBONATIC CLAYS. *International journal for numerical and analytical methods in geomechanics*, 549-574.

Laloui, L. (2010). *Mechanics of Unsaturated Geomaterial.* Hoboken, USA: John Wiley & Sons.

Laloui, L., & Cekerevac, C. (2003). Thermo-plasticity of clays: an isotropic yield mechanism. *Computers and Geotechnics*, 649-660.

Laloui, L., & Francois, B. (2006). A THM stress-strain framework for modelling the performance of argillaceous materials in deep repositories for radioactive waste. *Mont Terri 10 Years Anniversary Workshop*, (pp. 5-8). St-Ursanne.

Lambe, T., & Whitman, R. (1969). *Soil Mechanics.* New York, Singapore, Chichster: John Wiley & Sons.

Lancellotta, R. (2008). *Geotechnical Engineering.* London: CRC Press.

Li, H., Chen, M., Fu, B., & Liang, B. (2019). Evaluation on the thermal and moisture diffusion behavior of sand/bentonite. *Applied thermal engineering*, 55-65.

Lignau, B., Graham, J., Yarachewski, D., Tanaka, N., & Gray, M. (1996). Effects of temperature on strength and compressibility of sand-bentonite buffer. *Engineering geology*, 103-115.

Littleton. (1976). An experimental study of the adhesion between clay and steel. *journal of terramechanics*, 141-152.

Littleton, I. (1976). An experimental study of the adhesion between clay and steel. *Journal of terramechanics*, 141-152.

Lloret, A., Romero, E., & Villar, M. (2005). *FEBEX II Project Final Report on thermo-hydro-mechanical laboratory tests.* Madrid, Spagna: Enresa.

Lloret, A., Villa, M., Sanchez, M., Gens, A., Pintado, X., & Alonso, E. (2003). Mechanical behaviour of heavily compacted bentonite under high suction changes. *Geotechnique*, 27-40.

Lupin, O., Smart, N., Zhang, Z., Stefanoni, M., Angst, U., Papafotiou, A., & Diomidis, N. (2021). Anaerobic corrosion of carbon steel in bentonite: An evolving interface. *Corrosion science*.

Marschall, P., Giger, S., De La Vassiere, R., Shao, H., Leung, H., Nussbaum, C., . . . Alcolea, A. (2017). Hydro-mechanical evolution of the EDZ as transport path for radionuclides and gas: insights from the Mont Terri rock laboratory (Switzerland). *Swiss Journal Geoscience*, 173-194.

Martin, P., Barcala, J., & Huertas, F. (2006). Large-scale and long-term coupled thermo-hydro-mechanic. *Journal of Iberian Geology*, 259-282.

Michalec, Z., Blaheta, R., Hasal, M., & Ligursky, T. (2021). Fully coupled thermo-hydro-mechanical model with oversaturation and its validation to experimental data from FEBEX experiment. *International Journal of Rock Mechanics & Mining Science*, 139.

Michales, Z. B. (2021). Fully coupled thermo-hydro-mechanical model with oversaturation and its validation to experimental data from FEBEX experiment. *International journal of rock mechanics and mining science*.

Muhammad, N., & Siddiqua, S. (2022). Calcium bentonite vs sodium bentonite: The potential of calcium bentonite for soil foundation. *Materials today: proceedings*, 822-827.

Nuth, M., & Laloui, L. (2008). Effective stress concept in unsaturated soils: Clarification and validation of a unified framework. *Internation journal for numerical and analytical methods in geomechanics*, 771-801.

Oscarson, D., & Choi, J.-W. (1996). diffusive transport through compacted Na- and Ca-bentonite. *journal of contaminant hydrology*, 189-202.

Porcino, D. F. (2003). Interface behaviour of sands from constant normal stiffness direct shear tests. *Geotechnical Testing Journal*, 289-301.

Porcino, D., Fiorvante, V., Ghionna, V., & Pedroni, S. (2003). Interface Behavior of Sands from Constant normal stiffness direct shear tests. *Geotechnical Testing Journal*, 289-301.

Robinet, J. T.-M. (2021). Hydro-mechanical response of crushed argillite and bentonite mixtures as sealing material. *Engineering geology*.

Robinet, J., Tyri, D., & Djeran-Maigre, I. (2021). Hydro-mechanical response of crushed argillite and bentonite mixtures as sealing material. *Engineering Geology*, 288.

Romero, E. (2001). Controlled Suction techniques. *4° Simposion Brasileiro de Solos Nao Saturados* (pp. 535-542). Porto Alagre, Brasil: Gehiling & F. Schnaid.

Romero, E., & Vaunat, J. (2000). Retention curves of deformable clays. *Experimental Evidence and Theoretical Approaches in Unsaturated Soils*, 91-106.

Salager, S., Nuth, M., Ferrari, A., & Laloui, L. (2013). Investigation into water retention behaviour of deformable soils. *NCR research press*, 200-208.

Seiphoori, A., Ferrari, A., & Laloui, L. (2014). Water retention behaviour and microstructural evolution of MX80 bentonite during wetting and drying cycles. *Geotechnique*, 721-734.

Su, L., Zhou, W., Chen, W., & Jie, X. (2018). Effects of relative roughness and mean particle size on the shear strength of sand-steel interface. *Measurment*, 339-346.

Sun, D., Matsuoka, H., Morichi, K., Tanaka, Y., & Yamamoto, H. (2003). frictional behaviour between clay and steel by direct shear type apparatus. *Deformation characteristics of geomaterials*, 239-245.

Sun, D., Sun, W., & Fang, L. (2014). Swelling characteristics of Gaomiaozi bentonite and its prediction. *journal of rock mechanics and geotechnical engineering*, 113-118.

Takayama, Y., Tachibana, S., Iizuka, A., Kawai, K., & Kobayashi, I. (1027). Constitutive modeling for compacted bentonite buffer materials as unsaturated and saturated porous media. *Soils and foundations*, 80-91.

Tan, W. L. (2008). Behaviour of clay-steel interface. *int conf construct build technol*, 11-20.

Tang, G. X. (1999). *Suction characteristics and elastic-plastic modelling of unsaturated sand-bentonite mixture.* Winnipeg, Manitoba.

Tsubakihara, Y., & Kishida, H. (n.d.).

Tsubakihara, Y., & Kishida, H. (1993). Frictional behaviour between normally consolidated clay and steel by two direct shear type apparatuses. *Soils and foundations*, 1-13.

Tsunakihara, Y., Kishida, H., & Nishiyama, T. (1993). FRICTION BETWEEN COHESIVE SOILS AND STEEL. *Soils and foundations*, 145-156.

Tuttolomondo, A., Ferrari, A., & Laloui, L. (2021). Generalized effective stress concept for saturated active clays. *Canadian Science publishing*, 1627-1639.

Uesugi, M., & Kishida, H. (1986). frictional resistance at yield between dry sand and mild steel. *Soils and foundations*, 139-149.

Uesugi, M., & Kishida, H. (1986). influencial factors of friction between steel and dry sand. *Soils and foundations*, 33-46.

Valderrama, C., Gimenez, J., Pablo, D., J., & MArtinez, M. (2011). transport of strontium through a ca-bentonite and compaison with MX-80 Na-bentonite: experimental and modelling. *Water air soil pollut*, 471-478.

Vanapalli, S., Fredlund, D., Pufahi, D., & Clifton, A. (1996). Model for the prediction of shear strength with respect to soil suction. *Canadian Geotechnical Journal*, 379-392.

Villar, M. (1999). Investigation of the behaviour of bentonite by means of suction-controlled oedometer tests. *Engineering Geology 54*, 67-73.

Villar, M., & Lloret, A. (2008). Influence of dry density and water content on the swelling of a compacted bentonite. *Applied Clay Science*, 38-49.

Ye, W., Xu, L., Chen, B., Chen, Y., Ye, B., & Cui, Y. (2014). An approach based on two-phase flow phenomenon for modeling gas migration in saturated compacted bentonite. *Engineering geology*, 124-132.

Ye, W.-M., Zhang, Y., Chen, B., Zheng, Z., & Cui, Y.-J. (2012). Investigation on compression behaviour of highly compacted GMZ01 bentonite with suction and temperature control. *nuclear engineering and design*, 11-18.

Zhang, Z., Ye, W., Liu, Z., Wang, Q., & Cui, Y. (2020). Mechanical behaviour of GMZ bentonite pellet mixtures over a wide suction range. *Engineering geology* , 264.

Zheng, L., Samper, J., & Montenegro, L. (2011). A coupled THC model of the FEBEX in situ test with bentonite swelling and chemical and thermal osmosis. *Journal of contaminant hydrology*, 45-60.

Label	Test	duration	σ_v [kPa]	ρ [g/cm^3]	rate [mm/min]	τ_{max} [kPa]	τ_{ult} [kPa]	ψ_0 [kPa]	T_0 [°C]	w_0 [%]	ψ_f [kPa]	T_f [°C]	w_f [%]
T130_100	1	3h20min	1000	1.36	0.05	97.56	93.73	133.77	nd	nd	135.59	Nd	Nd
T130_200	2	-	200	-	-	193.72	183.49	127.22	nd	Nd	127	Nd	Nd
T130_500	3	-	500	-	-	442.16	426.29	133.49	Nd	Nd	134.82	Nd	nd
T130_1000	4	-	1000	-	-	789.22	734.31	137.89	Nd	Nd	138.7	Nd	Nd
T130_1500	5	-	1500	-	-	918.86	847.38	137.43	Nd	Nd	140.81	Nd	Nd
T130_2000	6	-	2000	-	-	1238.1	1211.04	137.43	nd	Nd	130.58	Nd	Nd
T130_1000_2	7	-	1000	-	-	816.48	802.31	134.01	22.8	6.75	130.58	23.3	6
T130_1000_3	8	-	1000	-	-	721.69	682.56	132.7	23.1	5.21	132.01	23.3	5.82
T130_2000_2	9	-	2000	-	-	1250.8	1129.14	129.55	23.5	5.31	131.17	23.8	5.86
T130_1500_2	10	-	1500	-	-	992.09	941.29	134	22.8	6	135.04	23.1	6.03
T130_2000_3	11	-	2000	-	-	1297.56	1167.18	128.44	22.6	5.77	129.54	23.3	5.78
T130_200_2	12	-	200	-	-	199.18	198.04	128.89	23.2	6.04	128.29	23.6	5.7
T130_500_2	13	-	500	-	-	427.29	408.62	126.73	22.7	6.13	128.08	23.1	6.09
T130_200_3	14	-	200	-	-	169.44	160.56	128.3	22.7	6.1	128.09	23.2	5.88
T130_1000_4	15	-	1000	-	-	752.56	703.54	132.12	22.3	5.77	133.03	22.9	5.93
T130_1000_5	16	-	1000	-	-	722.05	682.11	131.78	22.9	5.6	133.55	23.1	5.68
T130_1500_3	17	-	1500	-	-	1024.26	982.05	132.02	22.9	5.94	133.04	23	5.82
T130_500_3	18	-	500	-	-	419.12	398.67	131.46	23	5.75	133.72	23.1	5.77
TT_1000	19	3h20min	1000	nd	-	646.13	540.17	64.97	nd	nd	71.3	nd	Nd
TT_1000_2	20	5h20min	1000	nd	-	745.89	727.45	181.02	Nd	Nd	174.02	Nd	Nd
TT_1000_3	21	3h20min	1000	Nd	-	734.82	680.64	71.56	Nd	Nd	83.52	Nd	Nd
TT_1000_4	22	5h20min	1000	Nd	-	770.22	757.54	58.03	22.9	11.72	58.5	23.2	10.91
TT_1000_5	23	-	1000	Nd	-	619.44	606.84	35	23.3	12.34	46	23.5	11.44
TT_1000_6	24	4h20min	1000	nd	-	605.8	599.9	40.8	22.6	12.7	45.8	23.2	12.54
T40_100	25	5h20min	100	1.13	-	105.59	105.59	39.34	22.4	12.56	44.98	22.7	12.3
T40_200	26	5h30min	200	-	-	248.39	242.97	42.64	23	12.68	44.87	23.5	12.38
T40_500	27	-	500	-	-	411.96	392.08	38.78	22.8	13.05	46.68	23.2	12.42
T40_1000	28	5h50min	1000	-	-	619.25	550.49	37.6	23.1	12.98	41.38	23.9	12.50

Appendix

T16_200	29	5h45min	200	0.99	-	211.30	199.27	16.03	22.6	16.23	21.06	23.5	16.50
T16_500	30	5h40min	500	-	-	342.31	321.60	15.39	22.6	16.46	19.02	23.5	16.28
T16_1000	31	-	1000	-	-	506.63	442.60	16.72	22.4	16.13	19.97	22.3	17.65
T40_100	32	5h15min	100	1.13	-	141.59	137.8	44.52	22.9	11.71	47.08	23.6	11.37
T40_1500	33	5h20min	1500	-	-	770.88	629.38	44.6	22.9	11.64	47.08	23.6	11.68
T16_100	34	4h15min	100	0.99	-	149.82	146.37	16.26	23.6	16.46	17.94	23.8	16.63
T16_1500	35	4h20min	1500	-	-	584.86	504.52	15.68	22.7	16.94	18.70	23.5	16.77
T16_1000_2	36	5h15min	1000	-	-	470.4	385.04	16.98	23.3	16.38	19.44	23.6	16.14
I130_200	37	3h15min	200	1.36	-	110.78	98.05	125.31	23.6	6.21	121.19	24.1	5.58
I130_500	38	-	200	-	-	216.68	200.66	126.26	23.8	5.4	122.36	24	5.52
I130_1000	39	-	500	-	-	413.14	368.19	117.05	23.3	5.62	119.95	23.8	5.62
I130_100	40	3h30min	100	-	-	61.53	52	124.02	23.3	6	124.17	23.6	5.8
I130_1500	41	-	1500	-	-	533.63	461.28	119.4	23.6	5.8	117.78	23.8	6
I15_100	42	5h20min	100	0.99	-	60.74	55.46	14.81	23.2	17.7	16.58	23.6	17.3
I15_200	43	-	200	-	-	100.4	88.25	15.28	23.6	17.2	16.29	23.3	17.3
I15_500	44	-	500	-	-	208.4	185.83	15.18	23.1	17.5	17	23.5	16.9
I15_1000	45	5h15min	1000	-	-	420.72	368.19	15.46	23.6	16.62	20.48	24.4	16.41
I15_1500	46	5h20min	1500	-	-	551.26	458.22	15.82	23.3	17.3	18.17	23.5	17.1
I130_1500_2	47	3h20min	1500	1.36	-	545.58	519.65	119.65	23.6	5.9	119.07	23.8	5.9
I130_1000_3	48	-	1000	-	-	383.60	354.86	117.03	23.8	5.9	116.24	24.2	5.8
I130_500_2	49	-	500	-	-	204.09	185.68	107.78	23.9	6.3	105.67	24.3	6.1